

A COMPARATIVE ANALYSIS OF THE ADSORPTION AND FRACTIONATION OF RARE EARTH
ELEMENTS ON KAOLINITE, Palygorskite, Montmorillonite,
AND SYNTHETIC CLAY MINERALS

by

Natalie Catherine Rose

© Copyright by Natalie Catherine Rose, 2023

All Rights Reserved

A thesis submitted to the Faculty and the Board of Trustees of the Colorado School of Mines in partial fulfillment of the requirements for the degree of Master of Science (Geology and Geochemistry).

Golden, Colorado

Date _____

Signed: _____

Natalie Catherine Rose

Signed: _____

Dr. Richard F. Wendlandt
Thesis Advisor

Golden, Colorado

Date _____

Signed: _____

Dr. Wendy A. Bohrson
Department Head
Department of Geology

ABSTRACT

Knowing the geochemical behavior of rare earth elements (REE) in clay mineral-dominated systems is essential to understanding observed REE fractionation in clay-hosted REE deposits. Previous work has focused on the behavior and distribution coefficients ($\log K_d$) of single REE on individual clay minerals and do not have the ability to show fractionation of REE. Testing if fractionation is driven by processes involving clay minerals requires systematic study of adsorption behaviors for REE as a function of varying clay mineral properties.

In this study, four Clay Mineral Society source clays, kaolinite (KGa-1), palygorskite (PFl-1), Na-montmorillonite (SWy-2), and synthetic mica-montmorillonite (Ba-SYn-1), selected on the basis of their surface areas and cation exchange capacities (CEC), were reacted with REE-enriched fluids to determine the $\log K_d$ of each REE-clay mineral combination. The REE used in the study, Nd, Gd, and Yb, represent light, middle, and heavy portions of the lanthanide series. Each clay mineral was also equilibrated with a REE mix to evaluate REE fractionation. Adsorption isotherms were determined using purified and size-fractionated clay minerals at 1-atm pressure, constant $T = 25^\circ\text{C}$ and pH that was buffered between 6.4-7.3. All adsorption isotherms followed the Freundlich equation.

Measured $\log K_d$ values, defined as the concentration ratio $\text{clay}_{\text{REE}}/\text{aqueous phase}_{\text{REE}}$, are the same for individual REE and for KGa-1, PFl-1, and SWy-2, ranging from 1.42 to 2.75. $\log K_d$ values for Ba-SYn-1 are higher, at 2.73, but do not vary between the REE. When REE are in competition, KGa-1 shows a slight preference for the heavier REE: $\log K_d$ for Nd is 2.01-2.57; $\log K_d$ values for Gd and Yb are 1.74-2.54. Other clay minerals show no fractionation of the REE mix.

The results of this study represent an internally consistent set of REE distribution coefficients obtained under identical conditions as well as data regarding the fractionation of REE on different clays. With the possible exception of Nd on kaolinite, the results of this study show that the observed fractionation of REE in clay mineral dominated environments is not attributable to clay mineral type, surface area, or CEC, but rather some other property of a weathering profile.

TABLE OF CONTENTS

ABSTRACT	iii
LIST OF FIGURES	vi
LIST OF TABLES	viii
ACKNOWLEDGMENTS	x
DEDICATION	xi
CHAPTER 1 INTRODUCTION AND BACKGROUND	1
1.1 Current State of Knowledge	1
1.2 Research Objectives	2
CHAPTER 2 MATERIALS AND METHODS	3
2.1 Clay Minerals	3
2.1.1 Selection Based on Specific Properties	3
2.1.2 Preparation of Pure Materials	4
2.1.3 Documentation of Purity	6
2.2 REE and Solutions	7
2.2.1 Selection and Specific Properties	7
2.2.2 Experiment Solution Preparation	8
2.3 Experiments and Analyses	9
2.3.1 Experimental Method	9
2.3.2 Analytical Methods	10
2.4 Data Analysis Methods	10
CHAPTER 3 RESULTS	13
3.1 Individual REE-Clay Couples	13
3.1.1 Kaolinite	13
3.1.2 Palygorskite	14
3.1.3 Montmorillonite	15

3.1.4	Ba-SYn-1	16
3.2	Individual REE-Clay Couple Values	17
3.3	Multiple REE-Clay Mineral Couples	18
3.3.1	Mixed REE	19
3.4	Mixed REE-Clay Couple Values	20
CHAPTER 4 DISCUSSION		22
CHAPTER 5 SUMMARY AND RECOMMENDATIONS FOR FUTURE WORK		25
REFERENCES		27
APPENDIX A RAW DATA		29
APPENDIX B TIME STUDY AND RANGE STUDY		45
B.1	Introduction	45
B.2	Numerical Modeling	45
B.3	Experimental Design	46
B.4	Hypothesis	46
B.5	Results	46
B.6	Conclusions	47
APPENDIX C CLAY MINERAL PREPARATION		48
C.1	Introduction	48
C.2	KGa-1	48
C.3	PFl-1	48
C.4	SWy-2	49
C.5	Ba-SYn-1	50

LIST OF FIGURES

Figure 2.1	Graphical comparison of clay minerals used in this study in terms of surface area and cation exchange capacities (CEC).	4
Figure 2.2	Flow chart detailing the sequence of operations involved with sample preparation through data analysis.	5
Figure 2.3	From top to bottom, KGa-1 < 2 μ m XRD Pattern, PFl-1 < 2 μ m XRD Pattern, SWy-1 > 5 μ m < 2 μ m XRD Pattern, Ba-SYn-1 < 2 μ m XRD Pattern	7
Figure 3.1	The left three plots represent the isotherm for the kaolinite and REE systems where log q_{REE} is the surface excess of REE on kaolinite as a function of log C_{REE} which is the concentration of Nd in solution. The right three plots represent the distribution coefficient (log K_d) as a function of concentration (C_{REE})	14
Figure 3.2	The left three plots represent the isotherm for the palygorskite and REE systems where log q_{REE} is the surface excess of REE on palygorskite as a function of log C_{REE} which is the concentration of Nd in solution. The right three plots represent the distribution coefficient (log K_d) as a function of concentration (C_{REE})	15
Figure 3.3	The left three plots represent the isotherm for the montmorillonite and REE systems where log q_{REE} is the surface excess of REE on montmorillonite as a function of log C_{REE} which is the concentration of Nd in solution. The right three plots represent the distribution coefficient (log K_d) as a function of concentration (C_{REE})	16
Figure 3.4	The left three plots represent the isotherm for the Ba-SYn-1 and REE systems where log q_{REE} is the surface excess of REE on Ba-SYn-01 as a function of log C_{REE} which is the concentration of Nd in solution. The right three plots represent the distribution coefficient (log K_d) as a function of concentration (C_{REE})	17
Figure 3.5	The left figure represents the relationship between surface excess (log q_{REE}) and concentration (log C_{REE}) of each REE on kaolinite while in competition. The right figure displays the relationship between the distribution coefficient (log K_d) and the concentration of REE (C_{REE})	19
Figure 3.6	The left figure represents the relationship between surface excess (log q_{REE}) and concentration (log C_{REE}) of each REE on palygorskite while in competition. The right figure displays the relationship between the distribution coefficient (log K_d) and the concentration of REE (C_{REE})	19
Figure 3.7	The left figure represents the relationship between surface excess (log q_{REE}) and concentration (log C_{REE}) of each REE on montmorillonite while in competition. The right figure displays the relationship between the distribution coefficient (log K_d) and the concentration of REE (C_{REE})	20
Figure 3.8	The left figure represents the relationship between surface excess (log q_{REE}) and concentration (log C_{REE}) of each REE on Ba-SYn-1 while in competition. The right figure displays the relationship between the distribution coefficient (log K_d) and the concentration of REE (C_{REE})	20

Figure 4.1 The left figure compares the $\log K_d$ with the cation exchange capacity of each REE on each clay mineral while the right compares the $\log K_d$ with surface area of each REE on each clay mineral 24

Figure B.1 This figure represents two components of the time study, a series of differing total amounts of Yb representing a constant time, 24 hours, and a constant total Yb over different times: 12, 24, and 36 hours to best understand when a reaction has reached completion 47

LIST OF TABLES

Table 2.1	Properties of clay minerals used in experiments	4
Table 2.2	Summary of REE properties	8
Table 3.1	A summary of the isotherm constants A and B for each clay mineral-REE pair. The constant A represents the capacity for the couple to adsorb while B represents the intensity of the adsorption	18
Table 3.2	A summary of the log distribution ($\log K_d$) coefficients for individual clay mineral-REE pairs	18
Table 3.3	A summary of the isotherm constants A and B for each clay mineral REE mix pair. The constant A represents the capacity for the couple to adsorb while B represents the intensity of the adsorption	20
Table 3.4	A summary of the log distribution coefficients ($\log K_d$) for mixed clay mineral-REE mix pairs	21
Table 4.1	Distribution coefficient equations for each mineral-REE pair	22
Table 4.2	A summary of the distribution coefficient equation for the log distribution ($\log K_d$) coefficients for individual clay mineral-mixed REE pair curves	23
Table 4.3	R squared goodness of fit values for each mineral-REE pair	23
Table 4.4	A summary of the R-squared goodness of fit for the log distribution ($\log K_d$) coefficients for individual clay mineral-mixed REE pair curves	23
Table A.1	Kaolinite-Neodymium Raw Data	29
Table A.2	Kaolinite-Gadolinium Raw Data	30
Table A.3	Kaolinite-Ytterbium Raw Data	31
Table A.4	Kaolinite-Mixed REE Raw Data	32
Table A.5	Palygorskite-Neodymium Raw Data	33
Table A.6	Palygorskite-Gadolinium Raw Data	34
Table A.7	Palygorskite-Ytterbium Raw Data	35
Table A.8	Palygorskite-Mixed REE Raw Data	36
Table A.9	Montmorillonite-Neodymium Raw Data	37
Table A.10	Montmorillonite-Gadolinium Raw Data	38
Table A.11	Montmorillonite-Ytterbium Raw Data	39

Table A.12	Montmorillonite-Mixed REE Raw Data	40
Table A.13	Ba-SYn-1-Neodymium Raw Data	41
Table A.14	Ba-SYn-1-Gadolinium Raw Data	42
Table A.15	Ba-SYn-1-Ytterbium Raw Data	43
Table A.16	Ba-SYn-1-Mixed REE Raw Data	44

ACKNOWLEDGMENTS

This thesis was written in many living rooms, bedrooms, kitchens, and computer labs in a variety of cities in a handful of countries, through numerous life situations, across the better part of a decade. Due to this, the task of detailing everyone who got me to the finish line would almost certainly take a document as long as this thesis itself.

None of what was done here could have been done without the constant enduring support of my advisor, Dr. Richard Wendlandt, and the encouragement of my mother, Allison. Further thanks go to all of those whose living rooms I occupied while making this happen and for anyone who ever took the time to be the wind in my sails when I needed it most.

Finally, special thanks go to my aunt, Joanne Hendrick, and my late grandfather, Roy Hendrick, and his wife, Lani Hendrick for providing the financial support to keep at this project for so long.

For everyone that answers the call to investigate the vast unknowns in this amazing universe we call home.

CHAPTER 1

INTRODUCTION AND BACKGROUND

Studies by Galán et al. (2007), Murakami and Ishihara (2008), and Sanematsu et al. (2009) have shown that weathering profiles and other clay mineral-based systems have the potential to concentrate and fractionate REE [1–3]. While elements such as lead and copper adsorb more readily than REE into available adsorptive sites on clay minerals in weathering profiles, REE have been observed to compete for these spots despite their larger atomic radii [4–6]. Although ideas have been advanced to explain why REE can become concentrated on clay mineral in weathering profiles despite competition from other elements, a thorough geochemical treatment of the processes potentially leading to the fractionation of REE on clay minerals remains elusive [1, 6, 7].

1.1 Current State of Knowledge

Previous research dealing with REE adsorption on clay minerals focuses on the geochemical reaction of trace element heavy brines interacting with clay minerals on the seafloor. Beall et al. (1976) and Aja (1998) attempted to recreate these reactions experimentally by introducing trace element laden brines to purified clay minerals in order to determine the distribution coefficient ($\log K_d$) of each reaction [5, 6]. While these papers are helpful in establishing the parameters and methods of adsorptive experiments, the heightened salinity of these experiments prevents their rigorous applicability to weathering profiles[5].

Beall et al. (1976) determined that REE adsorption is enhanced at neutral pH values and low salinities [6]. They found, as a general rule, that clay minerals with higher cation exchange capacities (CECs) and surface areas have increased adsorptive capacities. This behavior is not surprising given that a clay mineral with more surface sites and higher negative layer charge would preferentially adsorb REE relative to clay minerals without those properties. Comparative studies that focused on multiple REE such as Beall et al. (1976) were not able to identify differences in adsorptive potential for the lanthanide suite of elements within these brines [6].

It is known that the geochemical properties of REE are very similar, but it is unknown if these similarities preclude any variations in adsorption behavior and, thus, fractionation. Indeed, separation of REE in industrial REE processing involves repeated use of solvent extraction to slowly leach out the desired REE from the rest of the suite [8]. Due to the intense nature of REE processing, finding deposits that have already fractionated REE is one of the primary goals of REE prospect exploration [9]. Based on a comprehensive survey of lateritic supergene REE deposits Cocker (2012) documented that REE

resources, such as Mountain Pass and the deposits in Southeast Asia tend to be naturally enriched in restricted portions of the REE suite e.g. the lighter or heavier REE [9]. For instance, Mountain Pass is enriched with respect to the light REEs, including neodymium, that are used in magnets for high technology application [9]. In most occurrences where selective enrichment of REE is documented, the controlling factor is the initial crystalline composition of the host rock.

Within the clay- and laterite-hosted REE deposits in Southeast Asia and Spain, the observed REE distribution within the unweathered protolith does not match the REE concentrations in the clay minerals that are mined [1, 2]. Murakami and Ishihara (2008) propose that part of the reason for this fractionation is the repeated adsorption and de-adsorption of REE within the weathered portion of the deposit, however this explanation does not explicitly preclude small geochemical differences between the elements or the clay mineral assemblage being the cause [2].

1.2 Research Objectives

The objective of this study is to generate by experiment a set of internally-consistent $\log K_d$ values and adsorption isotherm equations for individual clay mineral-REE pairs that allows testing the hypothesis that individual clay mineral surface area, surface charge, and exchange site properties result in measurably different REE distribution coefficients and fractionation behaviors. The values will be comparable because all experimental data would be obtained for a consistent set of experimental conditions.

Given the diverse range of geochemical properties present in the clay minerals selected for this study, it is hypothesized that there will be measurably different the $\log K_d$ values and adsorption isotherms of each REE on a given clay mineral. Because larger CECs and surface areas provide more available sites for adsorption, the clay minerals that have higher values of these properties will have higher ability to adsorb REE and, thus, experimentally determined $\log K_d$ values and isotherm constants for individual REE will be larger compared to clay minerals with decreased CECs and surface areas.

Another objective of this study is to determine whether or not clay minerals can fractionate REE. This ability will be determined by reacting a blend of several REE with each clay mineral and determining the $\log K_d$ values and adsorption isotherm equations for the clay mineral-mixed REE couple. If the $\log K_d$ values for each REE within the mix are similar, it can be determined that the REE are not being fractionated by the clay mineral.

CHAPTER 2

MATERIALS AND METHODS

It was important to be able to select materials for this study that would highlight the variety of properties present in different clay minerals and REE in order to highlight the differences in adsorptive capacity for those clay minerals.

2.1 Clay Minerals

The term clay mineral refers to a wide variety of minerals made up of repeating layers of charged sheets. Due to differing sheet compositions, different clay minerals exhibit a variety of geochemical properties that can affect the ability for materials to adsorb to them. Given the varying geochemical properties of clay minerals, it was critical for this study to select clay minerals for their diverse properties.

2.1.1 Selection Based on Specific Properties

This study used four different clay minerals to examine the effects of varying clay mineral structure and layer charge on REE-adsorption. Table 2.1 and Figure 2.1 summarize the surface area and layer charges that characterize the clay minerals used in the experiments. The clay minerals used were chosen specifically to give a range of differing properties.

Kaolinite is a 1:1 layer type clay mineral that is comprised of one octahedral (O) layer attached to a tetrahedral (T) layer [10]. These units repeat with very little chemical substitution, which leads to both a low layer charge and a low surface area. Kaolinite is typically an end point for extreme chemical weathering. The surface area of the kaolinite was determined by the EGME method as detailed in Cerato and Luttenegger (2002) while the CEC was determined via the ammonia-electrode method as detailed by Borden and Giese (2001) [11, 12].

Palygorskite is a fibrous clay mineral with a 2:1 layer structure (T-O-T) that is composed of long, narrow strips that are connected at the edge tetrahedral sites to create internal channels [10]. These narrow channels are the primary location of cation adsorption. The surface area of the palygorskite was determined by the EGME method as detailed in Cerato and Luttenegger (2002) while the CEC was determined via the ammonia-electrode method as detailed by Borden and Giese (2001) [11, 12].

Montmorillonite is a 2:1 clay mineral structure type that has the ability to expand in the presence of water [10]. As montmorillonite expands it maintains the characteristic layered structure of clay minerals but the expansion allows for the inclusion of cationic species into the interlayer space leading to very high

CEC and surface area. The surface area of the montmorillonite was determined by the EGME method as detailed in Cerato and Luttenegger (2002) while the CEC was determined via the ammonia-electrode method as detailed by Borden and Giese (2001) [11, 12].

Ba-SYn-1 is a synthetic montmorillonite, with the same structure and properties as natural montmorillonite. Since Ba-SYn-1 is created synthetically, the clay mineral is pure and the particle size is homogenous. The surface area of Ba-SYn-1 was determined by the EGME method as detailed in Cerato and Luttenegger (2002) while the CEC was determined via the ammonia-electrode method as detailed by Borden and Giese (2001) [11, 12].

Table 2.1 Properties of clay minerals used in experiments [11–14]

Clay Mineral	ID	CEC (meq/100g)	SA (m ² /g)	Clay Fraction Utilized (μm)
Kaolinite	KGa-1	2.00	15	<2
Palygorskite	PFl-1	19.50	341	>0.1 <2
Montmorillonite	SWy-1	76.40	781	<2
Barium Ba-SYn-1	Ba-SYn-1	70.00	133.66	<2

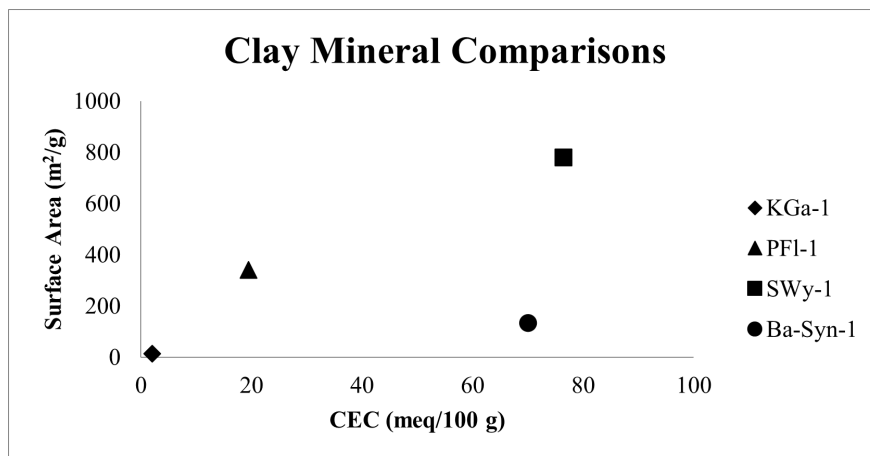


Figure 2.1 Graphical comparison of clay minerals used in this study in terms of surface area and cation exchange capacities (CEC). [11–14]

2.1.2 Preparation of Pure Materials

In order to obtain internally consistent and usable experimental results, it is critical to have clay minerals that are free of contamination, well-characterized, and homogenous. Aja (1998), Beall et al. (1976), and Chipera and Bish (2001) controlled clay mineral variables such as clay mineral purity, particle size, and surface site availability [5, 6, 13]. Accordingly, to produce experimental results that would be of

use going forward, the clay mineral sample preparation for this project focused on controlling these same variables.

The clay minerals used in this research represent a range of CEC values which relate to the surface site availability, surface areas, and clay mineral structures; due to these differences, each clay mineral was processed in a different manner in order to maximize its available adsorptive sites. Due to the intensive nature of processing that was required, sample preparation took place over several months. Figure 2.2 shows the sequence of steps involved with sample preparation and continuing through the experiments and data analysis. Appendix C further documents the creating of clay mineral samples for this study.

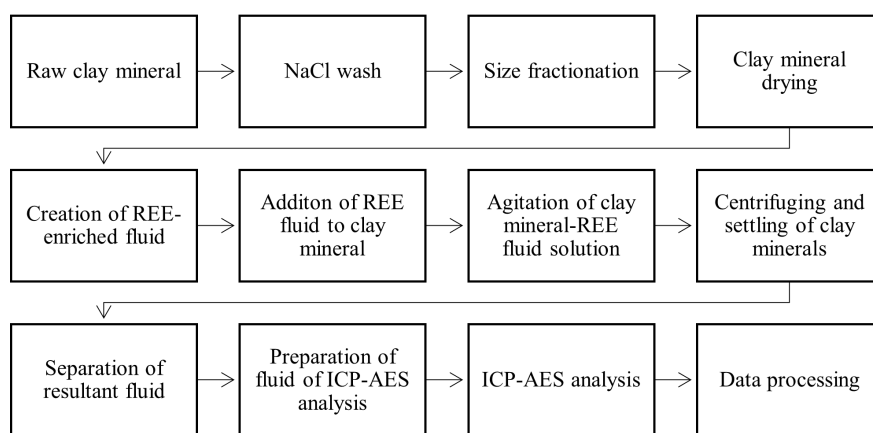


Figure 2.2 Flow chart detailing the sequence of operations involved with sample preparation through data analysis.

All clay minerals started off with a NaCl wash to saturate all clay exchangeable sites with Na^+ and remove other constituents that would compete with the REE solution during the adsorption experiments. The NaCl wash was 1.2 M NaCl solution. Samples were agitated in the NaCl solution for 48 hours at 20°C in a constant temperature bath.

Clay samples were then rinsed with DI water, centrifuged to settle suspended clay mineral particles, drained, and rinsed again. The rinse cycle was repeated three time until the decanted waste fluid did not visibly react with a silver nitrate solution. This method is analogous to that used by Chipera and Bish (2001) to obtain pure clay mineral samples [13].

The next treatment was to remove impurities and generate a controlled size fraction for each clay mineral. The KGa-1 that was used in this study has been the subject of many experimental studies and, thus, its purity has been assessed and was determined to meet the standards for this study. Following the NaCl wash and rinsing, DI water was added to each sample tube and each sample was centrifuged to settle

all suspended kaolinite to the bottom of the tubes. The supernatant was decanted, and the kaolinite was allowed to dry at 20°C for a week. The dried sample was stored in a sealed and acid washed container until used in experiments.

The palygorskite was subjected to a more intensive process due to the impurities that were known to be in PFl-1. In line with Chipera and Bish (2001), the size fraction between 0.1 and 2 μm was selected for this study to avoid the presence of large impurities outside this size range and to remove an extremely fine grain size montmorillonite impurity [13]. The desired size fraction was dried at low temperature and stored in a sealed and acid washed container until used.

The montmorillonite used for this project required extensive processing due to the high percentage of impurities that are present in SWy-2 and other Wyoming bentonites [15]. Since montmorillonite expands in the presence of the DI water used in this study, only small amounts of the clay mineral could be processed at a time. By combining gravimetric and mechanical separation methods, purified montmorillonite was obtained. Initially, the fraction larger than 2 μm was removed leaving a mixture of montmorillonite and impurities. As the montmorillonite underwent expansion in the presence of water, it became less dense and could be mechanically separated from the impurities that did not expand. The resulting size fraction was then dried at low temperature and then stored in a sealed and acid washed container until used in experiments.

The synthetic montmorillonite used in this study (Ba-SYn-1) is manufactured and contains a boehmite impurity due to the use of the mineral gibbsite in the manufacturing process [16]. While the exact procedure is proprietary, the synthesis of Ba-SYn-1 is completed at low temperature and residual boehmite is considered non-reactive to the Ba-SYn-1 [17]. In concert with other investigations that used Ba-SYn-1, including Cenens and Schoonheydt (1988), the boehmite was not removed from their Ba-SYn-1 samples prior to use in our experiments [18]. As was done for the other clay minerals prepared for this study, the Ba-SYn-1 was suspended in DI water and centrifuged to concentrate the $< 2 \mu\text{m}$ fraction. The resultant Ba-SYn-1 size fraction was dried at low temperature and stored in sealed and acid washed vials until used in experiments.

2.1.3 Documentation of Purity

Following the drying of each clay mineral, the samples were disaggregated by grinding in an agate mortar and pestle until they were once again a powder. Small splits of each powder were then analyzed by X-ray diffraction to confirm the purity of each clay mineral sample. These scans are shown in Figure 2.3. As shown in Figure 2.3, the clay minerals used in this study were pure with the exception of the boehmite impurity in Ba-SYn-1 and a minor quartz impurity in PFl-1.

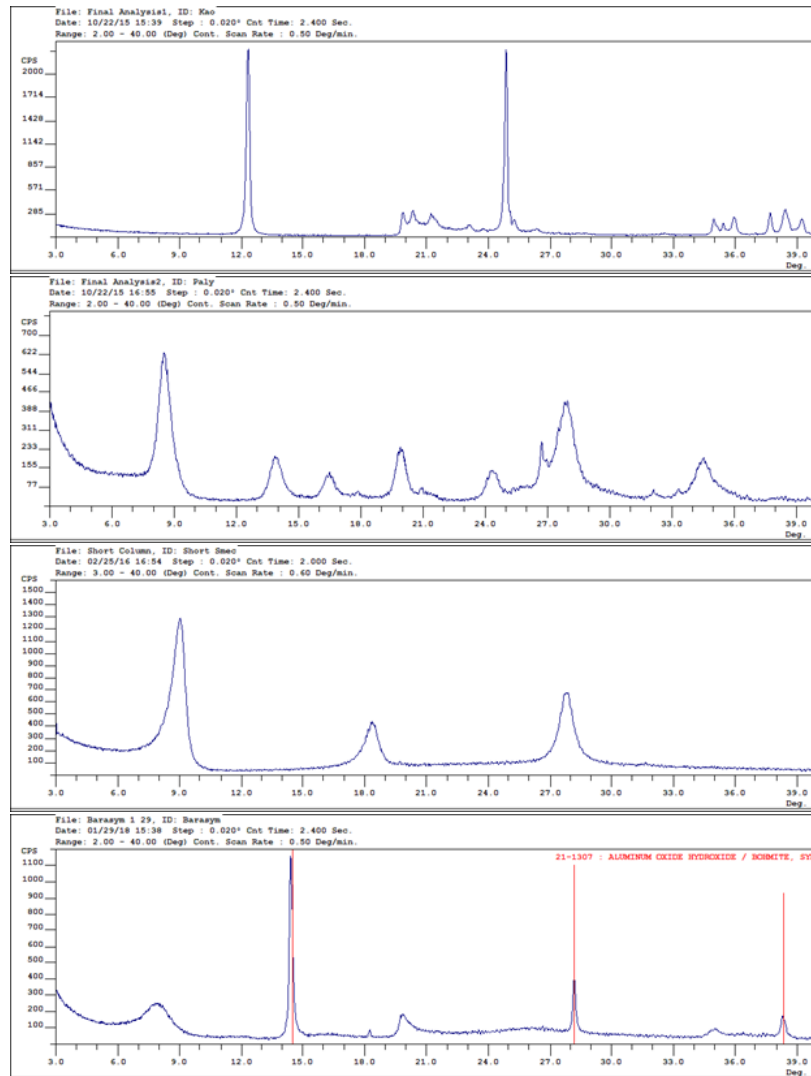


Figure 2.3 From top to bottom, KGa-1 < 2 μ m XRD Pattern, Pfl-1 < 2 μ m XRD Pattern, SWy-1 > 5 μ m < 2 μ m XRD Pattern, Ba-Syn-1 < 2 μ m XRD Pattern

2.2 REE and Solutions

REE represent a series of geochemically similar elements from lanthanum to lutetium that are used predominately in high tech applications. Due to their nearly homogenous geochemical properties, fractionating REE is a difficult process, and thus, selecting REE that represent the slightly different properties of the suite is critical to better understanding.

2.2.1 Selection and Specific Properties

The REE used for this study, neodymium, gadolinium, and ytterbium were selected as representatives for the light REE (LREE), middle REE (MREE), and heavy REE (HREE) respectively. Table 2.2 lists

pertinent properties that were considered for this study.

While there are other geochemical properties of REE that could affect a given REE's ability to adsorb onto clay minerals, the properties used in this selection represent the most fundamental properties and would serve as the easiest to compare.

Table 2.2 Summary of REE properties [19, 20]

Element	Ionic Radius (Å)	Charge	Electronegativity	Mass (g/mol)
Neodymium	1.175	+3	1.14	144
Gadolinium	1.105	+3	1.2	157
Ytterbium	1.010	+3	1.1	173

2.2.2 Experiment Solution Preparation

The REE-enriched fluids used in this study were prepared starting with calculating the concentrations needed to produce measurable $\log K_d$ values. The concentrations that were used were based on the assumption that the $\log K_d$ values would be constant once the adsorption sites were occupied by REE. Since Gibbs free energy would also limit the tendency for the REE to adsorb, it was decided that the final concentrations used for each clay mineral-REE experiment would be double the amount needed to fill the available surface sites as calculated from clay CECs. This excess concentration would be sufficiently high for analysis by ICP-AES. The maximum concentration was calculated using equations from Moore and Reynolds (1997), Langmuir (1997), Morel and Hering (1993) and Brown et al. (2006)[21–23]:

$$CEC = N_S \times S_A \times 0.1661 \quad (2.1)$$

$$N_S = \frac{CEC}{S_A \times 0.1661} \quad (2.2)$$

$$TOTS_A = S_A \times M_C \times 10^{18} \quad (2.3)$$

$$TOTN_S = TOTS_A \times N_S \quad (2.4)$$

$$mmolesREE = \frac{TOTN_S \times 10^3}{6.0221413 \times 10^{23}} \quad (2.5)$$

$$C_{REE} = \frac{mmolesREE}{V_{H_2O}} \quad (2.6)$$

where N_s is the number of sites per nm^2 of clay mineral, S_A is the surface area of the clay mineral, CEC is the cation exchange capacity of the clay mineral, $TOTS_A$ is the total surface area of the sample, M_C is the mass of the clay mineral, $TOTN_S$ is the total number of sites for the sample, and C_{REE} is the concentration of the reacting solution to be used.

The range of concentrations used in the experiment can be seen in the data presented in Appendix A. Each lower concentration was a fraction of the full concentration, the values of which were determined to

give a range over which the $\log K_d$ values and adsorption isotherms could develop. Following the initial experimental run it was found that the REE-enriched fluids had lower concentrations than initially planned, presumably due to REE precipitation during preparation. A second batch of REE-enriched fluid was created with higher available REE for adsorption. The process by which the two different REE-enriched fluids were created was identical besides for a difference in overall concentration ranges.

An analytical grade 10,000 ppm REE standard was used to create each REE-enriched fluid. These standards each contained a single REE and the concentration of REE in each standard was certified by the vendor.

The initial step in the creation of the REE-enriched fluids involved diluting the standard to the maximum calculated concentration for each clay mineral-REE couple. Each of these solutions was analyzed via ICP-AES to confirm that the sample had been prepared precisely. The pH was buffered to between 6.4 and 7.2 using sodium bicarbonate and each neutralized mixture was then partitioned into smaller aliquots representing each of the concentrations to be used in experiments. Once the REE solutions were added to an experiment, DI water was added to arrive at the desired concentration. The volumes of fluid were measured out using calibrated pipettes that were routinely tested to ensure their continued accuracy. Duplicate solutions were created at random in order to verify the results of experiments.

The production of the mixed REE solutions was similar to that used for the single REE solutions. The only difference was that the REE standards were used to create mixed solutions containing equal parts by concentration Nd, Gd, and Yb. These samples were treated in the same manner as the single REE solutions. Each mix was subjected to a sodium bicarbonate buffer that established a neutral pH.

2.3 Experiments and Analyses

Given that REE are geochemically similar, designing an experiment and choosing analytical methods that will result in higher resolution of the data is critical. By selecting the proper methods, worthwhile data can be achieved.

2.3.1 Experimental Method

Each concentration for the various clay mineral-REE couples was prepared individually. For the first series of experiments, 0.25 g of clay mineral was used in each mix. In the second series, 0.10 g was used. The difference in values came from the need to have less of each clay mineral to go with a higher REE concentration, thus decreasing the ratio of available surface sites to possible REE in solution. Each clay mineral sample was weighed out to five figures, although the overall specifications of the study only required three significant figures, thereby eliminating any calculable error stemming from the mass of each

clay mineral sample.

Following the weighing of each clay mineral sample, solids were mixed with the prepared REE-enriched fluid solutions to create a clay mineral-REE couple. These couples were then placed in a constant temperature agitation bath for 48 hours. This period of time had been determined to be sufficient to achieve a steady state with respect to REE adsorption based on a time study conducted prior to the main experiment. This time study is summarized in Appendix B and was part of the range-finding experiment that helped define the initial parameters of this study.

Following the completion of each experiment, samples were centrifuged to separate all of the clay mineral particles from the solution. The resultant fluid was pipetted out of the centrifuge tube and placed in new tubes and acidified with nitric acid to prepare the samples for the ICP-AES analysis.

The mixed REE experiments were conducted in the same fashion as the individual REE experiments.

2.3.2 Analytical Methods

The ICP-AES laboratory in the Department of Chemistry and Geochemistry, Colorado School of Mines, was used to conduct the analysis of all reacted REE solutions, duplicates, and DI water used in this study. The ICP-AES was chosen for analysis due to its sensitivity to REE and because the concentration ranges of the samples were within the machine's sensitivity range. Samples from batches of experiments were analyzed with lower concentration solutions preceding the higher ones. DI water was run between each set in order to determine the baseline REE concentrations detected by the ICP-AES. Samples were retrieved after analysis and stored for potential future analysis.

Results were returned in the form of spreadsheets that included data for all REE and several other trace elements. In order to best focus on the goals of this study, only the REEs that were investigated were run through the further analytical steps. This concentration limit was established through a time experiment that is detailed in Appendix B. The study primarily was concerned with figuring out at which point the experiments had reached equilibrium.

The method of ICP-AES analysis of the mixed REE solutions was similar to that of the individual REE solutions with the exception that these analyses were tested against mixed standards.

2.4 Data Analysis Methods

Analysis for this project was carried out in following steps with the goal of obtaining a $\log K_d$ value for each clay mineral-REE couple as well as the equations that best represent the obtained experimental data.

The preliminary step is to take the raw data output from the ICP-AES and process it through the following equations. This results in the $\log K_d$, $\log C_{REE}$, and $\log q_{REE}$. Plotting these data points

graphically results in the figures as seen in chapter three. These data points on their own show the observed progress of each adsorption reaction as they approach a stable state.

To obtain the values reported in the results, the data were processed as follows:

$$C_{REE} = C_{REE_{obsv}} \times \frac{V_i + V_a}{V_i} \quad (2.7)$$

$$q_{REE} = TOT_{REE} - Res_{REE} \quad (2.8)$$

$$K_{dREE} = \frac{q_{REE}}{C_{REE}} \quad (2.9)$$

$$LogK_d = Log_{10}(K_{dREE}) \quad (2.10)$$

$$LogC_{REE} = Log_{10}(C_{REE}) \quad (2.11)$$

$$Logq_{REE} = Log_{10}(q_{REE}) \quad (2.12)$$

where C_{REE} is the total concentration of the REE present during the reaction and $C_{REE_{obsv}}$ is the concentration of REE in the post-reaction solution as determined by the ICP-AES. These values are related by the total amount of fluid used in each experiment, including the initial volume of the REE-doped fluid V_i plus the volume of any added fluids V_a . The surface excess of REE on the clay mineral is q_{REE} while TOT_{REE} is the total REE available to react and Res_{REE} is the residual REE present after the reaction took place. $Log K_d$ is the distribution coefficient for each clay mineral-REE interaction.

The next step is to extrapolate the data forward to determine at what point the reactions are at a stable state. Determination of this approximate point involves ascertaining the style of each adsorption reaction and obtaining the A and B values for each isotherm, where for Freundlich equations, A and B represent the adsorptive capacity and intensity of each interaction respectively. Both parameters can be obtained both graphically, by plotting the $\log q_{REE}$ and $\log C_{REE}$ and determining the slope of each line, which is A, and the point where the slope intersects the $\log q_{REE}$ axis, as represented by B. These values are also checked numerically by a least squares method to determine a line of best fit for each clay mineral-REE couple.

$$q_{REE} = \log A + B \times \log C_{REE} \quad (2.13)$$

This leaves the determination of a stable $\log K_d$ for each couple. Sparks in 2003 and Singh in 2016 show that interactions between clay minerals and REE are governed by the Freundlich isotherm and the linear nature of each $\log C_{REE}$ and $\log q_{REE}$ back up this claim within the concentration ranges used [24, 25]. This means that the $\log K_d$ curve for each clay mineral-REE couple can be graphed logarithmically and by extrapolating that curve to the point at which each reaction has reach a stable level can be determined where the curve flattens out [5]. For some of the clay mineral couples, this stable level is evident visually from the data obtained while for others, the extrapolation is needed to determine this point.

Extrapolation of the data obtained is accomplished using a least squares analysis of the data to determine a logarithmic equation for each couple. Each equation is then tested with the R-squared method to determine goodness of fit for each curve with respect to the actual values.

CHAPTER 3

RESULTS

The following results represent two different approaches to determining the ability for REE to adsorb onto clay minerals. The experiment was designed to be able to give individual values associated with each REE-clay mineral couple as well as to give insight into how the different REE compete with each other for available surface sites on the clay minerals.

3.1 Individual REE-Clay Couples

Each individual REE-clay mineral couple is represented by two figures. The first figure is the surface excess, $\log q_{\text{REE}}$, as a function of the concentration of the REE in solution, $\log C_{\text{REE}}$. The slope of the curve can be interpreted to represent different styles of adsorption. The linear trends seen in this study, represent that the Freundlich isotherm is most applicable for interpreting the data in this experiment. Equations for each isotherm can then be determined by adding in the values A and B. The second figure in each set represents the distribution coefficient, $\log K_d$, as a function of concentration, C_{REE} .

3.1.1 Kaolinite

The initial calculations for KGa-1 anticipated that the clay mineral would have low distribution coefficients for each pair. This result was shown to be correct. Each of the $\log q_{\text{REE}} \log C_{\text{REE}}$ figures follows the linear trend that indicates the Freundlich isotherm is the appropriate adsorption model as seen in Figure 3.1.

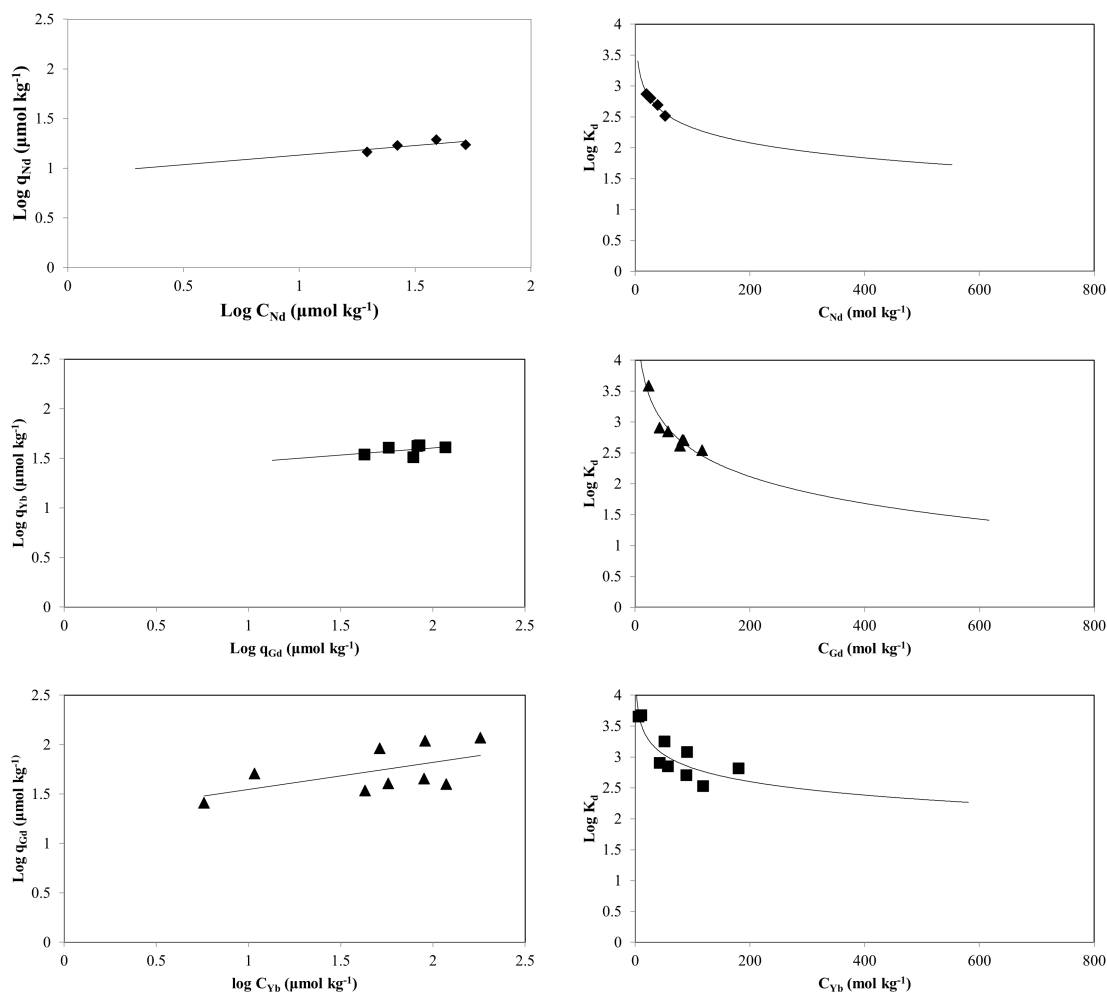


Figure 3.1 The left three plots represent the isotherm for the kaolinite and REE systems where $\log q_{REE}$ is the surface excess of REE on kaolinite as a function of $\log C_{REE}$ which is the concentration of Nd in solution. The right three plots represent the distribution coefficient ($\log K_d$) as a function of concentration (C_{REE})

3.1.2 Palygorskite

The analysis of the PFI-1-REE adsorption experiments confirms that the Freundlich isotherm is appropriate for the calculations of A and B in these systems. The excess number of samples for the neodymium-PFI-1 experiments show the relationship as concentration is increased as shown in Figure 3.2.

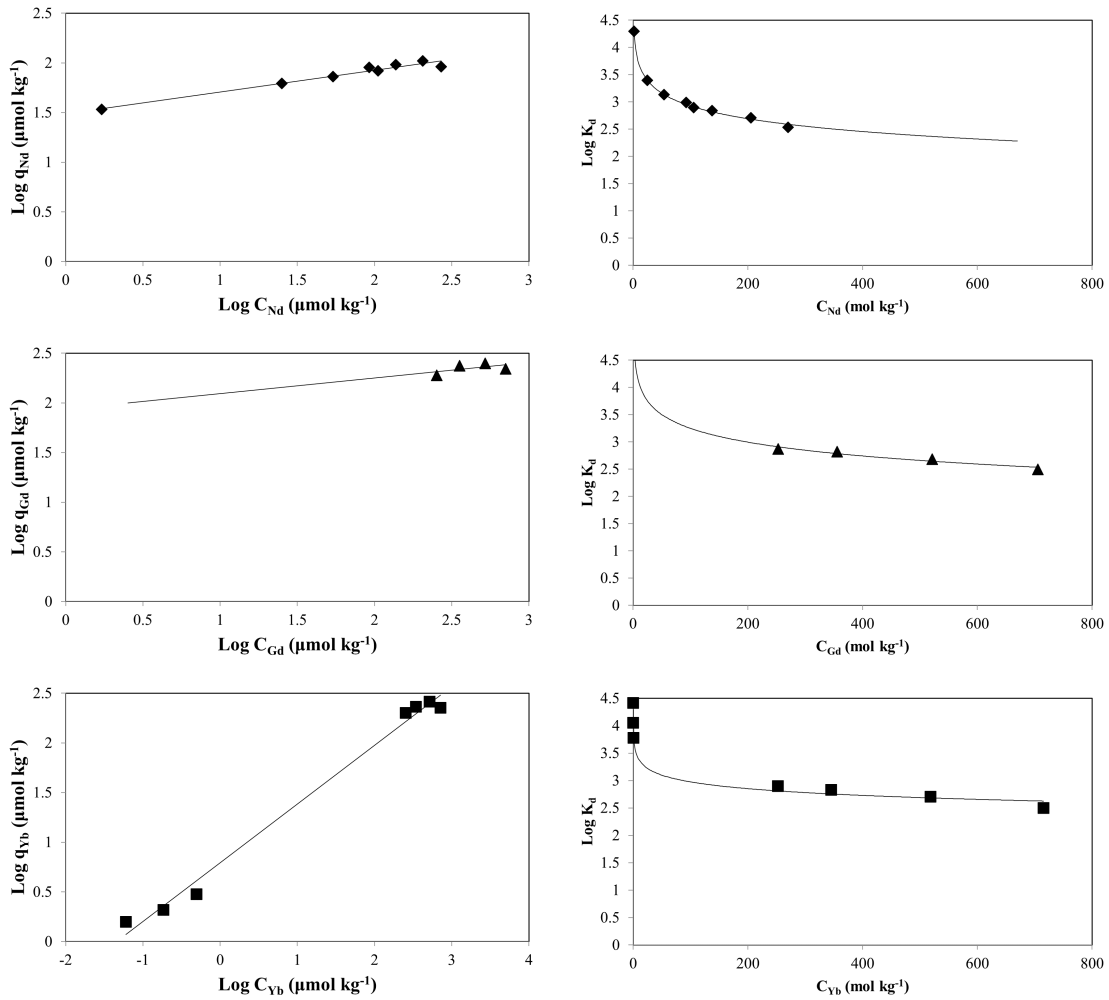


Figure 3.2 The left three plots represent the isotherm for the palygorskite and REE systems where $\log q_{\text{REE}}$ is the surface excess of REE on palygorskite as a function of $\log C_{\text{REE}}$ which is the concentration of REE in solution. The right three plots represent the distribution coefficient ($\log K_d$) as a function of concentration (C_{REE})

3.1.3 Montmorillonite

The SWy-1-REE couples continue the trend of REE-clay mineral couples being defined by the Freundlich isotherm. These trends are shown in Figure 3.3.

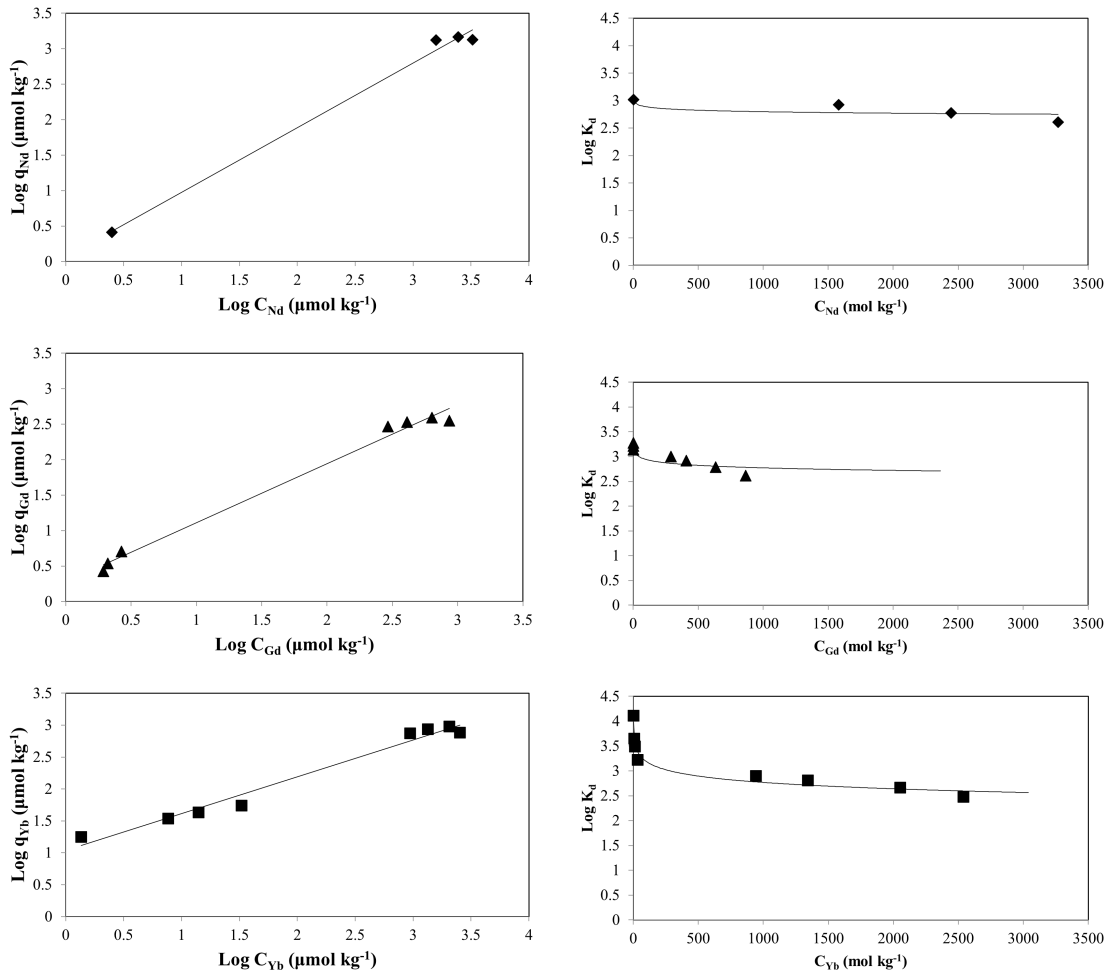


Figure 3.3 The left three plots represent the isotherm for the montmorillonite and REE systems where $\log q_{\text{REE}}$ is the surface excess of REE on montmorillonite as a function of $\log C_{\text{REE}}$ which is the concentration of Nd in solution. The right three plots represent the distribution coefficient ($\log K_d$) as a function of concentration (C_{REE})

3.1.4 Ba-SYn-1

The Ba-SYn-1-REE couples continue the trend of REE-clay mineral couples being defined by the Freundlich isotherm and show the most homogenous results of this study as shown in Figure 3.4.

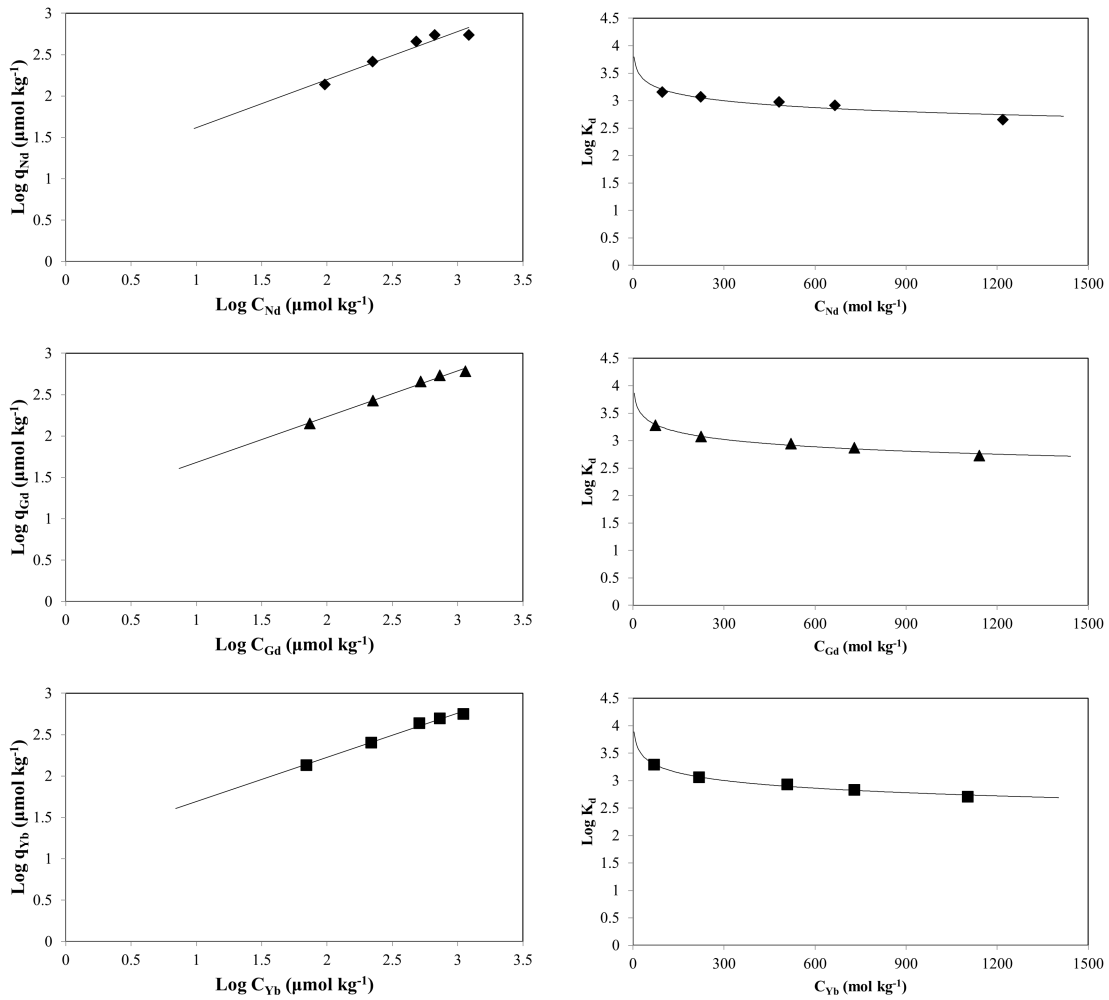


Figure 3.4 The left three plots represent the isotherm for the Ba-SYN-1 and REE systems where $\log q_{\text{REE}}$ is the surface excess of REE on Ba-SYN-01 as a function of $\log C_{\text{REE}}$ which is the concentration of Nd in solution. The right three plots represent the distribution coefficient ($\log K_d$) as a function of concentration (C_{REE})

3.2 Individual REE-Clay Couple Values

The distribution coefficients of each pair can be determined by taking the logarithmic equation for each $\log K_d$ curve and determining the value that the $\log K_d$ approaches. This value can then be compared with the values from other couple.

The data in Table 3.2 summarizes the distribution coefficients for each clay mineral/REE couple as calculated from the value that each curve approaches and documents that $\log K_d$ values generally increase with CEC and SA, at least for the sequence kaolinite < palygorskite < montmorillonite with Ba-SYN-1 serving as the exception. The similarity between the distribution coefficients for SWy-1 and Ba-SYN-1 when compared to their CEC and SA values indicates that the surface site availability is likely to have

greater influence on $\log K_d$ than SA.

This observation is further backed up by the coefficients for KGa-1 and PFl-1, though their similarities to the other values suggest that surface site availability is not the only determining factor.

Each set of coefficients for PFl-1, SWy-1, and Ba-SYn-1 follow a trend of the distribution coefficient increasing with atomic weight of the REE. KGa-1 varies from this and shows a more variable trend.

The A and B values for each couple, as shown in Table 3.1, show that a higher A, or adsorptive capacity of the clay mineral, is typically associated with a lower B, or intensity of adsorption for the REE on the clay mineral. For Swy-1 and Ba-SYn-1 these follow a trend toward lower A and higher B from the LREE to the HREE. KGa-1 and PFl-1 have much more variable A and B values.

Table 3.1 A summary of the isotherm constants A and B for each clay mineral-REE pair. The constant A represents the capacity for the couple to adsorb while B represents the intensity of the adsorption

Clay Mineral	Nd A	Nd B	Gd A	Gd B	Yb A	Yb B
Kaolinite	0.19	0.94	0.15	1.32	0.27	1.27
Palygorskite	0.22	1.24	0.16	1.93	0.59	0.79
Montmorillonite	0.98	-0.11	0.83	0.28	0.57	1.03
Ba-SYn-1	0.58	1.03	0.55	1.12	0.53	1.15

Table 3.2 A summary of the log distribution ($\log K_d$) coefficients for individual clay mineral-REE pairs

Clay Mineral	Neodymium	Gadolinium	Ytterbium
Kaolinite	1.70	1.42	2.25
Palygorskite	2.22	2.49	2.60
Montmorillonite	2.75	2.53	2.68
Ba-SYn-1	2.73	2.74	2.71

3.3 Multiple REE-Clay Mineral Couples

To better understand how REE compete for available surface sites on each clay mineral, REE-enriched fluids containing neodymium, gadolinium, and ytterbium in equal concentrations were allowed to react with the different clay minerals. Given that the REE were all present in equal concentrations, the distribution coefficients for each element could be obtained in the same manner as the single REE-clay mineral couples, but with the results modified by having the REE in competition, as they would be in a natural environment. Given both sets of distribution coefficients, the data from the mixed REE-clay mineral couples can be compared against the single REE-clay mineral couples to determine if competition changes adsorption behavior of any individual REE.

3.3.1 Mixed REE

The mixed REE-kaolinite couple indicates that kaolinite has the potential to preferentially adsorb LREE relative to HREE as shown in Figure 3.5. The higher distribution coefficient seen for Nd indicates that it will more readily adsorb onto the kaolinite.

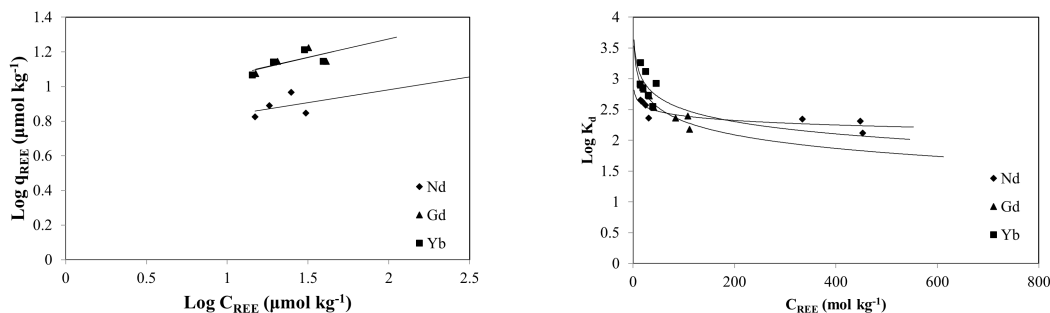


Figure 3.5 The left figure represents the relationship between surface excess ($\log q_{\text{REE}}$) and concentration ($\log C_{\text{REE}}$) of each REE on kaolinite while in competition. The right figure displays the relationship between the distribution coefficient ($\log K_d$) and the concentration of REE (C_{REE})

Given the similar curves for each REE on the palygorskite, it can be concluded that PFl-1 demonstrates no strong preference for a given REE as shown in Figure 3.6.

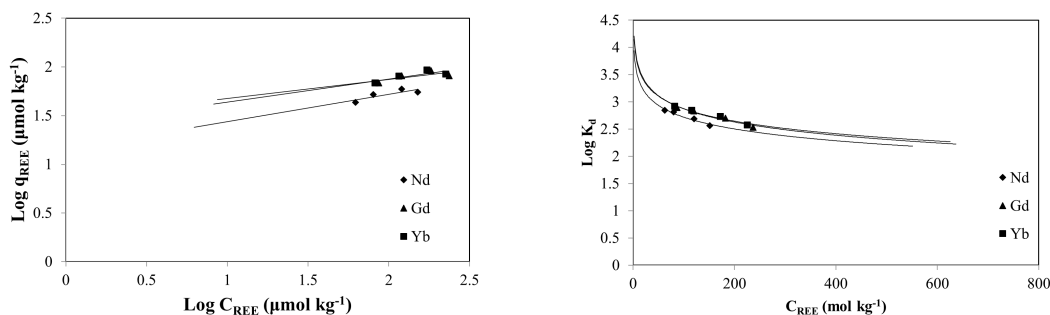


Figure 3.6 The left figure represents the relationship between surface excess ($\log q_{\text{REE}}$) and concentration ($\log C_{\text{REE}}$) of each REE on palygorskite while in competition. The right figure displays the relationship between the distribution coefficient ($\log K_d$) and the concentration of REE (C_{REE})

The distribution coefficient graph for the SWy-1-Mixed REE indicates a slight preference for Gd over Yb and Nd as shown in Figure 3.7.

The intriguing result of the Ba-SYn-1-Mixed REE couple is that the curves for both graphs are nearly identical, noticeably so for the distribution coefficient graph. This indicates that Ba-SYn-1 has equally strong preferences for all REE as shown in Figure 3.8.

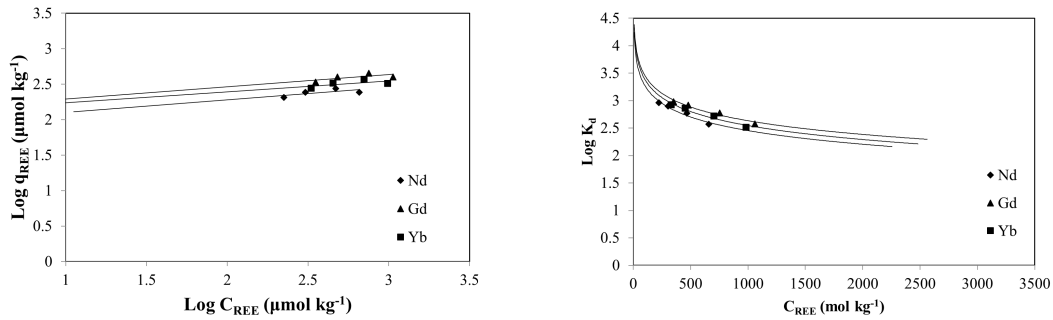


Figure 3.7 The left figure represents the relationship between surface excess ($\log q_{\text{REE}}$) and concentration ($\log C_{\text{REE}}$) of each REE on montmorillonite while in competition. The right figure displays the relationship between the distribution coefficient ($\log K_d$) and the concentration of REE (C_{REE})

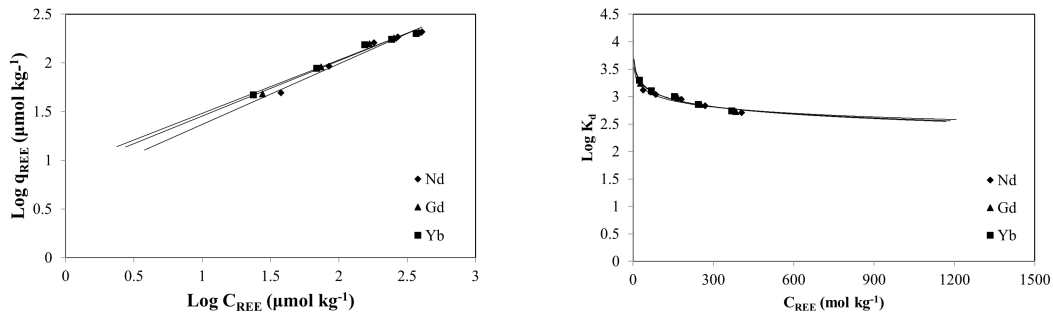


Figure 3.8 The left figure represents the relationship between surface excess ($\log q_{\text{REE}}$) and concentration ($\log C_{\text{REE}}$) of each REE on Ba-SYn-1 while in competition. The right figure displays the relationship between the distribution coefficient ($\log K_d$) and the concentration of REE (C_{REE})

3.4 Mixed REE-Clay Couple Values

The important information from Table 3.4 and Table 3.3 is that the clay minerals used in experiments show minimal tendency to fractionate REE when the REE are in competition, with the notable exception of Nd on KGa-1. By looking at these values compared with the individual couple results, it is evident that the $\log K_d$ values are less when in competition than when allowed to react individually.

Table 3.3 A summary of the isotherm constants A and B for each clay mineral REE mix pair. The constant A represents the capacity for the couple to adsorb while B represents the intensity of the adsorption

Clay Mineral	Nd A	Nd B	Gd A	Gd B	Yb A	Yb B
Kaolinite	0.15	0.69	0.21	0.85	0.21	0.85
Palygorskite	0.28	1.16	0.20	1.48	0.24	1.40
Montmorillonite	0.18	1.93	0.17	2.12	0.15	2.09
Ba-SYn-1	0.62	0.75	0.67	0.89	0.55	0.94

Table 3.4 A summary of the log distribution coefficients ($\log K_d$) for mixed clay mineral-REE mix pairs

Clay Mineral	Neodymium	Gadolinium	Ytterbium
Kaolinite	2.21	1.74	1.99
Palygorskite	2.07	2.14	2.19
Montmorillonite	2.01	2.18	2.08
Ba-SYn-1	2.57	2.54	2.53

CHAPTER 4
DISCUSSION

There are few published experimental studies having to do with mixed REE adsorption in adsorptive media. Since the suite of REE is present in most rocks and weathering profiles, studies that focus on the whole REE suite, as opposed to individual REE are critical for understanding the adsorptive capacity of a system. Most chondrite normalized analyses of weathering profile horizons show that there is at least some tendency for clay minerals and other weathering materials to fractionate REE relative to the parent rock (Sanematsu et al., 2009) [3]. In samples from clay-hosted REE deposits in Southeast Asia, the HREE tend to be present in higher concentrations within the soil horizons than would be expected if there had been no fractionation.

REE for this experiment had been chosen to represent the different atomic weights of the lanthanides. Other factors could also lead to more insight beyond what was obtained in this study. Cerium and europium both commonly have a different valence state than the rest of the REE and could show different results than the REE selected for this study. These valence variations vary more than the ionic radii and weights examined in this study and would have the potential to test whether chemical properties of REE would be more of a source of REE fractionation than the physical factors of the REE.

With the exception of kaolinite, which displays an adsorption preference for HREE, the measured K_d values obtained in the current study do not support REE fractionation involving palygorskite, montmorillonite or Ba-SYn-1. This is not a surprising conclusion due to the systematic variation of REE properties. Further, our results provide evidence that clay minerals with higher CEC and SA values adsorb more REE. Once again, this is not surprising since these factors would support stronger bonds and more adsorption sites.

Table 4.1 and Table 4.2 summarize the equations that define the curves for the single REE-clay mineral couples and the mixed REE-clay mineral couple as logarithmic functions.

Table 4.1 Distribution coefficient equations for each mineral-REE pair

Clay Mineral	Neodymium Equation	Gadolinium Equation	Ytterbium Equation
Kaolinite	$y=-0.35\ln(x)+3.940$	$y=-0.62\ln(x)+5.438$	$y=-0.31\ln(x)+4.272$
Palygorskite	$y=-0.34\ln(x)+4.489$	$y=-0.37\ln(x)+4.934$	$y=-0.18\ln(x)+3.793$
Montmorillonite	$y=-0.04\ln(x)+3.065$	$y=-0.18\ln(x)+4.038$	$y=-0.07\ln(x)+3.279$
Ba-SYn-1	$y=-0.18\ln(x)+4.032$	$y=-0.19\ln(x)+4.130$	$y=-0.20\ln(x)+4.157$

Table 4.2 A summary of the distribution coefficient equation for the log distribution ($\log K_d$) coefficients for individual clay mineral-mixed REE pair curves

Clay Mineral	Neodymium Equation	Gadolinium Equation	Ytterbium Equation
Kaolinite	$y=-0.11\ln(x)+2.888$	$y=-0.32\ln(x)+3.776$	$y=-0.29\ln(x)+3.829$
Palygorskite	$y=-0.31\ln(x)+4.157$	$y=-0.35\ln(x)+4.479$	$y=-0.33\ln(x)+4.40$
Montmorillonite	$y=-0.36\ln(x)+4.928$	$y=-0.36\ln(x)+5.118$	$y=-0.37\ln(x)+5.085$
Ba-SYn-1	$y=-0.16\ln(x)+3.746$	$y=-0.19\ln(x)+3.887$	$y=-0.20\ln(x)+3.936$

The applicability of these results can be determined through a statistical analysis of the $\log K_d$ values compared with each curve. Table 4.3 and Table 4.4 summarize the R squared goodness of fit values and indicates that with the exception of ytterbium on kaolinite, neodymium and gadolinium on montmorillonite, the $\log K_d$ values fit the data closely.

Table 4.3 R squared goodness of fit values for each mineral-REE pair

Clay Mineral	Neodymium R^2	Gadolinium R^2	Ytterbium R^2
Kaolinite	0.949	0.901	0.773
Palygorskite	0.997	0.935	0.981
Montmorillonite	0.559	0.804	0.959
Ba-SYn-1	0.872	0.984	0.987

Table 4.4 A summary of the R-squared goodness of fit for the log distribution ($\log K_d$) coefficients for individual clay mineral-mixed REE pair curves

Clay Mineral	Neodymium R^2	Gadolinium R^2	Ytterbium R^2
Kaolinite	0.751	0.933	0.315
Palygorskite	0.941	0.950	0.956
Montmorillonite	0.954	0.957	0.953
Ba-SYn-1	0.931	0.972	0.976

The R-squared values for each curve range from 0.750 to 1.000 with a few exceptions that show the limits of this study. The low value for neodymium on montmorillonite almost certainly is due to a low number of data points for that reaction, especially in the lower concentration range, which would allow for a better curve. The same problem is likely the source of the low R-squared value for Yb in the mixed REE experiments with kaolinite.

The only oddity in the data came from the palygorskite. Although palygorskite has higher surface site availability and SA than kaolinite by a factor of ten, it did not show comparably higher $\log K_d$ values for the REE. This discrepancy is tentatively explained by consideration of palygorskite's crystal structure,

which is a non-planar tubular shape. While the quantifiable effects of this structure are not fully evident, it is worth noting that this may explain the lower $\log K_d$ values for the REE-palygorskite couples.

Compared to the $\log K_d$ values obtained for the individual REE-clay mineral couples, those for the mixed REE couples are slightly depressed. This decrease is likely due to a weaker overall adsorption reaction intensity. For each set of mixed REE isotherm constants, A is similar to values from the individual REE results while B is significantly lower. This would result in a lower $\log K_d$ since the ability for the clay mineral to hold on to each REE is decreased.

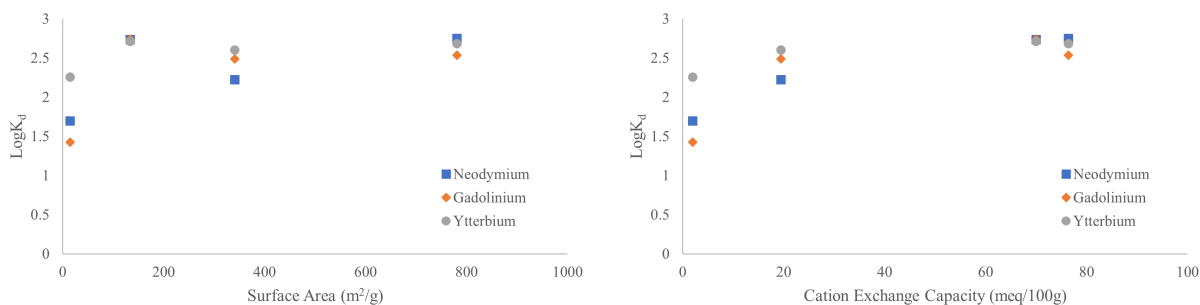


Figure 4.1 The left figure compares the $\log K_d$ with the cation exchange capacity of each REE on each clay mineral while the right compares the $\log K_d$ with surface area of each REE on each clay mineral

By comparing the $\log K_d$ values determined in this study to both the CEC and surface area as shown in Figure 4.1, it is clear that CEC is the primary control on REE adsorption onto the clay minerals selected. The higher the CEC of the clay mineral, the higher the observed $\log K_d$. This indicates that factors such as charge and valence would likely be the primary source of fractionation. Physical properties, such as surface area and ionic radius, are less important beyond serving as physical limits on the ability for REE to adsorb in the first place. Small scale variations in chemical properties of both the clay minerals and the REE are likely to be the predominate factor in why certain deposits have the ability to fractionate REE compared with others.

Within each REE mix, the values are similar indicating very little tendency for the clay minerals to fractionate the REE, at least on the scale tested in this study. Accordingly, it is likely that any fractionation of REE is driven by larger scale processes such as weathering at the rock-weathering profile interface or by movement of materials, both clay minerals and REE-enriched fluids within the weathering profiles. The data obtained from this study make clear that complex clay minerals with high cation exchange capacities have an increased capacity to adsorb the lanthanides, which is why deposits such as lateritic-hosted clay mineral deposits such as those in Southeast Asia are critical REE resources. Seeking out deposits with high-CEC clay minerals has the potential to provide more sources of REE.

CHAPTER 5

SUMMARY AND RECOMMENDATIONS FOR FUTURE WORK

It was found in this study that while there is little variation in the fractionation of REE on each clay mineral with the exception of kaolinite, which has a preference for HREE, there were significant differences in the $\log K_d$ values for each REE, likely arising from the different surface areas, available surface sites, and physical geometries of each clay mineral. Larger surface areas and available surface sites resulted in a higher ability for a clay mineral to adsorb REE. The only instance in this experiment where this was complicated was with palygorskite, which as noted above, does not have the planar structural geometry of the other clay minerals used.

Since there were no signs of fractionation in experiments conducted for this study beyond HREE on kaolinite, future work to establish the driving force behind the fractionation of REE within clay-hosted deposits should focus on other geochemical processes represented within the clay-hosted deposit. One possible place for this fractionation to happen is at the point of breakdown of the host rock. The formation of the lateritic layer within a weathering profile is a process consisting of both physical and chemical portions. Since the lateritic layer is the location of initial mobilization of REE within the weathering profile, it may be that some weathering processes allow for certain REE to be removed leaving behind more immobile REE within the laterite. While this process does not address heightened concentrations within clay-hosted deposits, it is an initial step.

A study to investigate this hypothesis could involve geological sampling across the vertical extent of a weathering profile, comparing the REE values of each phase within the weathering profile and analyzing the samples for their ability to adsorb and release REE. Studies such as Sanematsu et al. (2009) and Murakami and Ishihara (2008) have investigated the REE concentrations across a weathering profile, but these studies focus on ancient weathering profiles rather than active weathering profiles [2, 3]. By studying an active profile and analyzing the potential for each horizon within the profile to fractionate REE, the proposed study has potential to recognize where concentration and fractionation are occurring. Further, processes controlling REE fractionation could be investigated in the laboratory using different clay minerals and host rock systems. Such studies would be time and labor intensive but would contribute greatly to the established literature for both REE geochemistry and the geochemical processes within weathering profiles.

Given that this study only analyzed the fluids that remained after adsorption took place, a complementary study would be to directly quantify the adsorption of the REE on the clay minerals. Such a study would likely require stripping the REE off a variety of clay minerals of different grain size and

volume to establish a more constrained atomic mass balance. REE-enriched clay minerals could also be characterized via XRD and SEM to determine if any changes in mineralogy or mineral assemblage had taken place on a scale more deposit-encompassing than was investigated in this study. The goal of this approach would be to determine where in the weathering profile the REE are adsorbing onto the clay minerals surface. Such a study would be worth conducting provided that accurate and precise data could be obtained.

Another approach that would complement the findings in this paper would be to focus on systematically varying clay mineral properties rather than the REE. Since clay mineral adsorption can vary based on particle size, pH, and purity, it would be worth investigating how systematically controlling these properties affects the adsorption potential of a given clay mineral. A study designed in this manner would likely focus on a single clay mineral, such as the montmorillonite used in this study, and would attempt to identify how those clay mineral variables affect REE adsorption. Prior work, including that by Aja (1998) and Beall et al. (1976), characterized changes in $\log K_d$ as a function of changing pH; however, other variables were not controlled [5, 6]. In particular, the effects of varying particle size could be controlled and subjected to the same fractionation experiments that were the focus of the second part of this study to assess potential for REE fractionation.

REFERENCES

- [1] Galán E., Fernández-Caliani J.C., Miras A., Aparicia P., and Márquez M.G. Residence and fractionation of rare earth elements during kaolinization of alkaline peraluminous granites in nw spain. *Clay Minerals*, (42):341–352, 2007.
- [2] H. Murakami and S. Ishihara. Ree mineralization of weathered crust and clay sediment on granitic rocks in the sanyo belt, sw japan and the southern jiangxi province, china. *Resource Geology*, (58): 373–401, 2008.
- [3] K. Sanematsu, H. Murakami, Y. Watanabe, S. Duangsurigna, and S. Vilayhack. Enrichment of rare earth elements (ree) in granitic rocks and their weathered crusts in central and southern laos. *Bulletin of the Geological Society Survey of Japan*, (60):527–558, 2009.
- [4] W.Y. Wan Zuhairi, A.R. Samsudin, and T.B. Kong. The sorption distribution coefficient of lead and copper on the selected soil samples from selangor. *Bulletin of the Geological Society of Malaysia*, (54): 21–25, 2008.
- [5] S.U. Aja. The sorption of the rare earth element, nd, onto kaolinite at 25°c. *Clays and Clay Minerals*, (46):103–109, 1998.
- [6] G.E. Beall, B.H. Ketelle, R.G. Haire, and G.D. O’Kelley. Sorption behavior of trivalent actinides and rare earths on clay minerals, radioactive waste in geological storage. *ACS Symposium Series*, pages 201–213, 1976.
- [7] M.O. Barnett and D.B. Kent. Adsorption of metals by geomedia ii: Variables, mechanisms, and model applications. *Developments in Earth & Environmental Sciences*, (7), 2008.
- [8] Kidela Capital Group. Rare earth processing 101, 2011. URL www.kidela.com.
- [9] M.D. Cocker. Lateritic, supergene rare earth element (ree) deposits. *Arizona Geological Survey Special Paper*, (9), 2012.
- [10] D.M Moore and R.C. Reynolds. *X-Ray Diffraction and the Identification and Analysis of Clay Minerals*. Oxford University Press, 1997.
- [11] A.B. Cerato and A.J. Lutenegger. Determination of surface area of fine-grained soils by the ethylene glycol monoethyl ether (egme) method. *Geochemical Testing Journal*, (25), 2002.
- [12] D. Borden and R.F. Giese. Baseline studies of the clay minerals society source clays: cation exchange capacity measurements by the ammonia-electrode method. *Clays and Clay Minerals*, (49):444–445, 2001.
- [13] S.J. Chipera and D.L. Bish. Baseline studies of the clay minerals society source clays: powder x-ray diffraction analyses. *Clays and Clay Minerals*, (39):398–409, 2001.
- [14] J. Środoń and D.K. McCarty. Surface area and layer charge of smectite from cec and egme/h₂o-retention measurements. *Clays and Clay Minerals*, (56):155–174, 2008.

- [15] R.F. Wendlandt and W. Harrison. Surface coatings on quartz grains and their relevance to human health. *Applied Geochemistry*, (22):2290–2306, 2007.
- [16] W.T. Granquist. Synthetic silicate minerals. U.S. Patent 3,252,757A, issued May 24, 1966.
- [17] S.P. Mehrotra, T.C. Alex, G. Greifzu, and R. Kumar. Mechanical activation of gibbsite and boehmite: New findings and their implications. *Transactions of the Indian Institute of Metals*, (69), 2015.
- [18] J. Cenens and R.A. Schoonheydt. Visible spectroscopy of methylene blue on hectorite, laponite b, and barasym in aqueous suspension. *Clays and Clay Minerals*, (36):214–224, 1988.
- [19] P. D’Angelo, A. Zitolo, V. Migliorati, G. Chillemi, M. Duvail, P. Vitorge, S. Abadie, and R. Spezia. Revised ionic radii of lanthanoid (iii) ions in aqueous solution. *Inorganic Chemistry*, (50):4572–4579, 2011.
- [20] K. Li and D. Xue. Estimation of electronegativity of elements in different valence states. *Journal of Physical Chemistry A*, (110):11332–11337, 2006.
- [21] D. Langmuir. *Aqueous Environmental Geochemistry*. Prentice Hall, New Jersey, 1997.
- [22] F.M.M. Morel and J.G. Hering. *Principles and Applications of Aquatic Chemistry*. John Wiley & Sons, 1993.
- [23] T.L. Brown, H.E. Jr. LeMay, and B.E. Burnsten. *Chemistry, The Central Science*. Pearson Prentice Hall, 2006.
- [24] A.K. Singh. *Engineered Nanoparticles*. Academic Press, 2016.
- [25] D.L. Sparks. *Environmental Soil Chemistry*. Academic Press, 2003.

APPENDIX A

RAW DATA

The following data represent the raw concentrations in mg/L for each sample used in this experiment. The naming formula is clay initial (K for kaolinite, P for palygorskite, S for montmorillonite, and B for Ba-SYn-1) followed by REE initial (N for neodymium, G for gadolinium, Y for ytterbium, and M for REE mix). For palygorskite, montmorillonite, and Ba-SYn-1, samples 7 and 8 represent non-reacted fluids while the 1-6 represent fluid reacted with clay minerals. The fluids used for 7 and 8 for each sample were also used to calibrate the kaolinite samples.

Table A.1 Kaolinite-Neodymium Raw Data

C Mg/L	KN-1	KN-2	KN-3	KN-4	KN-5	KN-6	KN-7	KN-8
Ce 413.764	0.82259	0.97427	1.1132	1.61498	2.60474	3.39306	4.54816	6.17594
Dy 353.170	0.10008	0.10828	0.13158	0.18555	0.32011	0.41172	0.53461	0.766
Er 349.910	0.17892	0.19655	0.24317	0.35445	0.59861	0.77991	1.00897	1.43277
Eu 381.967	0.02317	0.02578	0.03104	0.0444	0.07978	0.10289	0.13478	0.19284
Gd 342.247	0.15344	0.17638	0.20484	0.283	0.4767	0.63579	0.815	1.17682
Ho 345.600	0.06857	0.07889	0.09425	0.13961	0.24002	0.31327	0.39844	0.57854
La 379.478	0.10104	0.10891	0.13448	0.19868	0.3395	0.45155	0.58201	0.84249
Lu 261.542	0.01229	0.01297	0.01586	0.02388	0.03731	0.04952	0.06487	0.09463
Nd 406.109	0.47868	0.55271	0.72181	1.11281	1.79452	2.3987	4.10947	5.3479
Pr 390.844	0.33135	0.36607	0.43485	0.65324	1.11085	1.54339	2.04389	2.75752
Sc 361.383	0.01431	0.01539	0.0187	0.02717	0.04925	0.06088	0.07746	0.11227
Sm 442.434	0.47345	0.56457	0.65891	0.96793	1.64381	2.11203	2.78816	3.83373
Tb 350.917	0.20937	0.2376	0.2822	0.40758	0.70375	0.92184	1.18927	1.71134
Th 283.730	BDL	BDL	0.44185	0.62786	1.10247	1.38582	1.83415	2.62392
Tm 346.220	0.10544	0.11284	0.14254	0.20595	0.34891	0.46022	0.58949	0.84883
Y 371.029	0.02352	0.02581	0.03031	0.04446	0.07632	0.09859	0.12699	0.18177
Yb 328.937	0.01226	0.01328	0.01673	0.02362	0.03941	0.0496	0.06343	0.09148
Clay Mass (g)	13.69561	14.01685	13.38151	13.86136	13.62785	13.84647	13.68311	14.15169

Table A.2 Kaolinite-Gadolinium Raw Data

C Mg/L	KG-1	KG-2	KG-3	KG-4	KG-5	KG-6	KG-7	KG-8
Ce 413.7	9.93186	10.79984	9.76823	9.77554	2.12888	3.57042	5.80647	6.56155
Dy 353.1	1.17651	1.28921	1.16107	1.17061	0.27654	0.51928	0.78698	0.87608
Er 349.9	2.2461	2.44867	2.22002	2.2364	0.53848	0.97514	1.46364	1.6415
Eu 381.9	0.29671	0.32556	0.29258	0.29566	0.07018	0.12499	0.1924	0.20949
Gd 342.2	1.81722	2.03652	1.87734	1.97135	0.57087	0.929	5.47671	4.99518
Ho 345.6	0.89414	0.98069	0.88238	0.89371	0.21064	0.3865	0.58597	0.65775
La 379.4	1.31329	1.43012	1.29076	1.2928	0.2924	0.53312	0.80737	0.89744
Lu 261.5	0.14515	0.15627	0.14024	0.14079	0.03636	0.05987	0.09578	0.10045
Nd 406.1	6.99308	7.61394	6.83848	6.87763	1.56395	2.71042	4.62196	5.05999
Pr 390.8	4.38666	4.82706	4.31786	4.35835	1.0685	1.78872	2.83512	3.21751
Sc 361.3	0.17209	0.18878	0.16994	0.1716	0.04682	0.07402	0.11493	0.12178
Sm 442.4	6.25557	6.8343	6.11731	6.17894	1.39082	2.38479	3.87168	4.40136
Tb 350.9	2.6861	2.94956	2.63693	2.6847	0.60758	1.10758	1.6963	1.87873
Th 283.7	3.93407	4.36343	3.91656	3.98113	0.81746	1.52287	2.2875	2.53615
Tm 346.2	1.32123	1.43707	1.31113	1.32425	0.32136	0.58453	0.88596	0.97908
Y 371.02	0.28629	0.31399	0.28183	0.28345	0.06713	0.117	0.17886	0.19643
Yb 328.9	0.14052	0.15443	0.13892	0.14122	0.03613	0.05987	0.09566	0.10373
Clay Mass (g)	13.87188	13.59117	13.42336	13.61199	13.19917	13.46145	13.96303	13.68087

Table A.3 Kaolinite-Ytterbium Raw Data

C Mg/L	KY-1	KY-2	KY-3	KY-4	KY-5	KY-6	KY-7	KY-8
Ce 413.7	9.3531	8.87515	11.84073	11.10588	15.5471	11.24461	17.49536	16.62939
Dy 353.1	1.21819	1.152	1.54402	1.43224	1.9816	1.49449	2.27979	2.16487
Er 349.9	2.2969	2.16796	2.92974	2.72125	3.75415	2.82658	4.31193	4.12705
Eu 381.9	0.2961	0.27941	0.37886	0.35122	0.48501	0.36357	0.55797	0.52827
Gd 342.2	1.78692	1.67505	2.26873	2.11225	2.89428	2.18535	3.33464	3.19507
Ho 345.6	0.90644	0.85783	1.16239	1.07274	1.47383	1.1282	1.70954	1.62759
La 379.4	1.26782	1.19996	1.61727	1.49221	2.06344	1.55901	2.37449	2.25947
Lu 261.5	0.13807	0.13075	0.17811	0.16361	0.21976	0.17357	0.25772	0.24655
Nd 406.1	7.05135	6.5695	8.8611	8.15834	11.63284	8.31365	13.07141	12.32997
Pr 390.8	4.58709	4.21279	5.64348	5.26708	7.33932	5.35085	8.30225	7.9298
Sc 361.3	0.16797	0.16153	0.21426	0.19924	0.27414	0.20587	0.31552	0.30002
Sm 442.4	6.36546	5.90095	7.99548	7.44002	10.54414	7.62564	11.8337	11.23701
Tb 350.9	2.65615	2.52574	3.40603	3.14199	4.34238	3.29259	5.00558	4.75559
Th 283.7	3.50819	3.37463	4.51517	4.26662	5.77021	4.44237	6.74003	6.32318
Tm 346.2	1.36516	1.28824	1.73759	1.60672	2.22693	1.68337	2.56289	2.43525
Y 371.02	0.27613	0.26144	0.35303	0.32834	0.45619	0.34579	0.52755	0.50065
Yb 328.9	0.15124	0.28257	1.35029	2.38533	4.78016	6.74119	10.72302	11.02639
Clay Mass (g)	13.85064	13.3487	13.11509	12.96793	13.3095	13.63423	13.69464	13.54695

Table A.4 Kaolinite-Mixed REE Raw Data

C Mg/L	KM-1	KM-2	KM-3	KM-4	KM-5	KM-6	KM-7	KM-8
Ce 413.7	9.9402	9.71755	9.97522	13.43135	13.38599	15.60554	15.77038	18.53669
Dy 353.1	1.29457	1.26763	1.32469	1.76151	1.73336	2.022	2.04636	2.41697
Er 349.9	2.43692	2.38106	2.49979	3.35899	3.29236	3.85456	3.89876	4.60156
Eu 381.9	0.31384	0.30773	0.32188	0.43019	0.42098	0.49613	0.50071	0.59363
Gd 342.2	1.88759	1.88184	2.02338	2.68029	2.59717	3.16106	3.43006	3.90442
Ho 345.6	0.96461	0.9424	0.99669	1.32811	1.29828	1.5238	1.54025	1.82344
La 379.4	1.3428	1.30738	1.36523	1.83919	1.79265	2.12016	2.1305	2.51169
Lu 261.5	0.14457	0.14379	0.1455	0.19765	0.19358	0.23081	0.22945	0.27657
Nd 406.1	7.43537	7.29115	7.36889	9.96095	9.86157	11.57889	12.12118	13.95288
Pr 390.8	4.75714	4.7301	4.75077	6.35596	6.35113	7.45738	7.56078	8.86462
Sc 361.3	0.17912	0.17489	0.18311	0.24383	0.2389	0.28037	0.28181	0.33337
Sm 442.4	6.7714	6.57942	6.71815	9.08851	8.89313	10.54052	10.72421	12.54832
Tb 350.9	2.82521	2.75604	2.88427	3.88391	3.81058	4.46156	4.4947	5.30917
Th 283.7	3.80647	3.70407	3.89731	5.24461	5.06736	5.9681	6.07522	7.17225
Tm 346.2	1.44865	1.41335	1.48112	1.98104	1.93508	2.28819	2.29375	2.71844
Y 371.02	0.29359	0.28652	0.29894	0.40211	0.39242	0.46394	0.46541	0.55277
Yb 328.9	0.1505	0.16949	0.38933	0.65045	1.20648	1.43669	2.53972	3.22893
Clay Mass (g)	13.92512	13.91412	13.99394	13.20392	13.35155	13.48302	13.82813	13.79625

Table A.5 Palygorskite-Neodymium Raw Data

C Mg/L	PN-1	PN-2	PN-3	PN-4	PN-5	PN-6	PN-7	PN-8
Ce 413.7	BDL	BDL	BDL	BDL	BDL	BDL	0.02197	0.00838
Dy 353.1	BDL	BDL	BDL	BDL	0.00494	0.00893	0.01399	0.02418
Er 349.9	BDL	BDL	BDL	BDL	0.00786	0.0103	0.02197	0.03334
Eu 381.9	BDL	BDL	0.00025	0.00236	0.00572	0.00995	0.01009	0.01974
Gd 342.2	BDL	BDL	BDL	BDL	BDL	BDL	0.00553	0.00227
Ho 345.6	BDL	BDL	BDL	BDL	BDL	BDL	0.00451	0.00318
La 379.4	BDL	BDL	BDL	0.00124	0.00895	0.01347	0.01778	0.03266
Lu 261.5	BDL	BDL	BDL	BDL	BDL	BDL	0.0003	BDL
Nd 406.1	BDL	0.03756	0.54994	1.18481	2.03749	3.40845	2.86373	6.02082
Pr 390.8	BDL	BDL	BDL	BDL	0.00708	0.00883	0.03666	0.05743
Sc 361.3	BDL	BDL	BDL	BDL	BDL	BDL	0.00234	0.00226
Sm 442.4	BDL							
Tb 350.9	BDL	BDL	BDL	BDL	BDL	BDL	0.00371	BDL
Th 283.7	BDL							
Tm 346.2	BDL	BDL	BDL	BDL	BDL	BDL	0.00386	BDL
Y 371.02	BDL	BDL	BDL	BDL	BDL	BDL	0.00174	0.0018
Yb 328.9	BDL	BDL	BDL	BDL	0.00026	0.00011	0.00115	0.00121
Clay Mass (g)	0.25136	0.25079	0.25099	0.25135	0.25151	0.25195	0	0

Table A.6 Palygorskite-Gadolinium Raw Data

C Mg/L	PG-1	PG-2	PG-3	PG-4	PG-5	PG-6	PG-7	PG-8
Ce 413.7	BDL	BDL	BDL	BDL	BDL	0.00551	BDL	0.20308
Dy 353.1	BDL	BDL	BDL	BDL	BDL	BDL	BDL	0.02337
Er 349.9	BDL	BDL	BDL	BDL	BDL	0.00293	BDL	0.04649
Eu 381.9	BDL	BDL	BDL	BDL	BDL	BDL	BDL	0.00555
Gd 342.2	BDL	BDL	BDL	BDL	0.00509	0.00795	0.1105	0.04871
Ho 345.6	BDL	BDL	BDL	BDL	BDL	0.00181	BDL	0.0193
La 379.4	BDL	BDL	BDL	BDL	BDL	BDL	BDL	0.02289
Lu 261.5	BDL	BDL	BDL	BDL	BDL	0.00021	BDL	0.00276
Nd 406.1	BDL	BDL	BDL	BDL	BDL	0.00381	BDL	0.14962
Pr 390.8	BDL	BDL	BDL	BDL	BDL	BDL	BDL	0.08986
Sc 361.3	BDL	BDL	BDL	BDL	BDL	BDL	BDL	0.00277
Sm 442.4	BDL	BDL	BDL	BDL	BDL	BDL	BDL	0.13847
Tb 350.9	BDL	BDL	BDL	BDL	BDL	0.00341	BDL	0.05458
Th 283.7	BDL	BDL	BDL	BDL	BDL	BDL	BDL	0.0837
Tm 346.2	BDL	BDL	BDL	BDL	BDL	0.00182	BDL	0.02776
Y 371.02	BDL	BDL	BDL	BDL	BDL	BDL	BDL	0.00531
Yb 328.9	BDL	BDL	BDL	BDL	BDL	0.00014	BDL	0.00275
Clay Mass (g)	0.25083	0.25	0.25042	0.2523	0.25029	0.25016	0	0

Table A.7 Palygorskite-Ytterbium Raw Data

C Mg/L	PY-1	PY-2	PY-3	PY-4	PY-5	PY-6	PY-7	PY-8
Ce 413.7	0.17141	0.04901	BDL	0.01271	0.01593	0.07772	0.04844	0.00864
Dy 353.1	0.02225	0.00815	0.00078	BDL	0.00379	0.0106	0.00783	0.00293
Er 349.9	0.04422	0.01858	0.00445	0.00302	0.01002	0.02337	0.01745	0.00852
Eu 381.9	0.00554	0.00172	BDL	BDL	0.00057	0.00213	0.0016	0.00028
Gd 342.2	0.03317	0.01331	0.00212	0.00249	0.00711	0.01874	0.01457	0.00663
Ho 345.6	0.01842	0.00743	0.00179	0.00213	0.00482	0.00908	0.00738	0.00392
La 379.4	0.0216	0.00766	BDL	BDL	0.00369	0.01164	0.00666	0.00201
Lu 261.5	0.00274	0.00117	0.00008	0.00014	0.0005	0.00135	0.00096	0.00039
Nd 406.1	0.1314	0.03229	BDL	0.0066	0.01661	0.05608	0.04053	0.00984
Pr 390.8	0.07866	0.00743	BDL	BDL	0.00363	0.0298	0.01946	BDL
Sc 361.3	0.00378	0.00103	BDL	BDL	BDL	0.00117	0.00074	BDL
Sm 442.4	0.11216	0.02202	BDL	BDL	0.00567	0.04332	0.0294	0.00568
Tb 350.9	0.05323	0.02124	0.00304	0.00265	0.01091	0.02711	0.02134	0.00766
Th 283.7	0.08542	BDL						
Tm 346.2	0.02597	0.01133	0.00212	0.00135	0.00584	0.01442	0.01187	0.00554
Y 371.02	0.00543	0.00172	BDL	BDL	0.0005	0.003	0.00178	0.00047
Yb 328.9	0.00305	0.00147	0.00163	0.00494	0.0132	1.20098	0.24369	0.17255
Clay Mass (g)	0.24486	0.25221	0.25771	0.25434	0.25368	0.25053	0	0

Table A.8 Palygorskite-Mixed REE Raw Data

C Mg/L	PM-1	PM-2	PM-3	PM-4	PM-5	PM-6	PM-7	PM-8
Ce 413.7	0.12198	0.07659	0.09774	0.0754	0.09953	0.16015	0.05891	0.10469
Dy 353.1	0.01843	0.01064	0.01363	0.01212	0.01527	0.02372	0.0098	0.01446
Er 349.9	0.03868	0.0228	0.03087	0.02531	0.03226	0.04845	0.02274	0.02996
Eu 381.9	0.00431	0.00245	0.00328	0.00246	0.00368	0.0055	0.00208	0.00337
Gd 342.2	0.03166	0.01646	0.02457	0.01865	0.02404	0.03805	0.02438	0.03001
Ho 345.6	0.01579	0.00912	0.0124	0.01025	0.01316	0.01902	0.00933	0.01291
La 379.4	0.01813	0.0103	0.01338	0.01165	0.01528	0.02446	0.00898	0.01379
Lu 261.5	0.0019	0.00122	0.00161	0.00159	0.00184	0.00247	0.00119	0.00128
Nd 406.1	0.09848	0.06853	0.08214	0.05109	0.0766	0.11514	0.05582	0.0784
Pr 390.8	0.05081	0.02687	0.04492	0.02136	0.04395	0.07039	0.01901	0.03359
Sc 361.3	0.00219	0.00202	0.00183	0.00143	0.00186	0.00305	0.001	0.0016
Sm 442.4	0.08071	0.0423	0.06907	0.03377	0.06219	0.09911	0.03651	0.05724
Tb 350.9	0.04387	0.02721	0.03417	0.02953	0.03672	0.05891	0.02589	0.0348
Th 283.7	0.07401	BDL	BDL	BDL	0.06573	0.09046	BDL	BDL
Tm 346.2	0.02248	0.01355	0.01728	0.01547	0.01942	0.0291	0.01352	0.01799
Y 371.02	0.00425	0.0025	0.00293	0.00251	0.00344	0.00557	0.00212	0.00325
Yb 328.9	0.00236	0.00168	0.00205	0.00206	0.0041	0.01044	0.0806	0.09689
Clay Mass (g)	0.25062	0.25398	0.25105	0.25179	0.25755	0.25408	0	0

Table A.9 Montmorillonite-Neodymium Raw Data

C Mg/L	SN-1	SN-2	SN-3	SN-4	SN-5	SN-6	SN-7	SN-8
Ce 413.7	0.05025	0.06724	0.05168	0.17221	0.19318	0.23165	0.25179	0.35745
Dy 353.1	0.00915	0.01051	0.01322	0.02531	0.0293	0.03181	0.03657	0.04313
Er 349.9	0.01896	0.0219	0.02837	0.05048	0.05684	0.06205	0.07057	0.08466
Eu 381.9	0.00165	0.00226	0.00291	0.00627	0.00685	0.00742	0.00864	0.01062
Gd 342.2	0.0147	0.01866	0.02148	0.04068	0.04459	0.04934	0.05613	0.06592
Ho 345.6	0.00759	0.00934	0.01165	0.02099	0.02334	0.02497	0.02863	0.03393
La 379.4	0.00756	0.00912	0.01286	0.02591	0.02887	0.0319	0.03576	0.04328
Lu 261.5	0.00084	0.00107	0.00163	0.00315	0.00339	0.0036	0.00397	0.00486
Nd 406.1	0.04629	0.05356	0.05475	0.13486	0.14696	0.20039	0.2212	0.28648
Pr 390.8	0.01718	0.02469	0.01932	0.07587	0.08771	0.09559	0.11486	0.15345
Sc 361.3	0.00078	0.00099	0.00139	0.00416	0.00388	0.00417	0.0046	0.00566
Sm 442.4	0.02786	0.03724	0.03209	0.10109	0.12415	0.14425	0.17475	0.22186
Tb 350.9	0.0217	0.02673	0.03402	0.06001	0.06766	0.07244	0.08498	0.10149
Th 283.7	BDL	BDL	BDL	0.09611	0.11028	0.12512	0.12044	0.14928
Tm 346.2	0.01311	0.01438	0.01699	0.03097	0.03476	0.03691	0.0422	0.04868
Y 371.02	0.00158	0.00224	0.00263	0.00598	0.00644	0.00691	0.00828	0.00996
Yb 328.9	0.00119	0.0014	0.00188	0.00371	0.00369	0.00386	0.00444	0.00519
Clay Mass (g)	0.25137	0.25128	0.25213	0.25228	0.2511	0.25253	0	0

Table A.10 Montmorillonite-Gadolinium Raw Data

C Mg/L	SG-1	SG-2	SG-3	SG-4	SG-5	SG-6	SG-7	SG-8
Ce 413.7	0.47832	0.20749	0.19558	0.2055	0.29218	0.1226	0.16013	0.26723
Dy 353.1	0.06317	0.02757	0.02862	0.03042	0.03951	0.02045	0.02583	0.03757
Er 349.9	0.11328	0.05596	0.05683	0.06007	0.07794	0.03995	0.05173	0.07266
Eu 381.9	0.01574	0.00661	0.00671	0.00708	0.00944	0.00475	0.00613	0.00878
Gd 342.2	0.0914	0.0438	0.04579	0.04978	0.06271	0.03401	0.16768	0.30117
Ho 345.6	0.04642	0.02328	0.0234	0.02402	0.03183	0.01656	0.02128	0.02915
La 379.4	0.06491	0.02844	0.02875	0.03023	0.04085	0.02017	0.0249	0.03684
Lu 261.5	0.00596	0.00308	0.00311	0.00297	0.00439	0.00265	0.00267	0.00419
Nd 406.1	0.37393	0.15595	0.14555	0.16264	0.21237	0.08674	0.12051	0.21362
Pr 390.8	0.2333	0.08729	0.08637	0.09127	0.13291	0.04565	0.07139	0.12643
Sc 361.3	0.00824	0.00342	0.00364	0.00386	0.00514	0.00347	0.0035	0.00507
Sm 442.4	0.3335	0.12776	0.12051	0.13157	0.18046	0.06598	0.10534	0.16211
Tb 350.9	0.13864	0.06614	0.06872	0.07139	0.09001	0.04664	0.05955	0.08739
Th 283.7	0.17165	0.10094	0.10261	0.1121	0.14239	0.07631	0.10104	0.13147
Tm 346.2	0.06522	0.03385	0.03455	0.03584	0.04653	0.0223	0.03132	0.04416
Y 371.02	0.01421	0.00639	0.0064	0.00671	0.00917	0.00447	0.00567	0.00829
Yb 328.9	0.00687	0.00337	0.00359	0.00378	0.00484	0.00282	0.00323	0.00452
Clay Mass (g)	0.25103	0.2517	0.24958	0.25148	0.24823	0.25221	0	0

Table A.11 Montmorillonite-Ytterbium Raw Data

C Mg/L	SY-1	SY-2	SY-3	SY-4	SY-5	SY-6	SY-7	SY-8
Ce 413.7	0.21936	0.23293	0.29376	0.28119	0.3491	0.39219	0.63246	0.52544
Dy 353.1	0.02621	0.03097	0.0397	0.03869	0.04711	0.05178	0.08168	0.06898
Er 349.9	0.05223	0.0597	0.07761	0.07571	0.08968	0.09803	0.15676	0.13217
Eu 381.9	0.00603	0.00696	0.00948	0.00922	0.01136	0.01254	0.02004	0.01737
Gd 342.2	0.04062	0.04709	0.0613	0.05976	0.07168	0.07931	0.12146	0.10591
Ho 345.6	0.02093	0.02467	0.03133	0.03094	0.03624	0.04033	0.0615	0.05439
La 379.4	0.02599	0.03011	0.03982	0.03916	0.04724	0.05332	0.08338	0.07051
Lu 261.5	0.00278	0.00317	0.00415	0.00428	0.00537	0.00577	0.00909	0.00853
Nd 406.1	0.14946	0.16235	0.20175	0.20978	0.25492	0.27966	0.45345	0.38008
Pr 390.8	0.0901	0.10288	0.12586	0.12759	0.15952	0.1736	0.28356	0.24066
Sc 361.3	0.00322	0.00393	0.00514	0.00503	0.00615	0.00685	0.01107	0.0103
Sm 442.4	0.13158	0.14387	0.17608	0.17685	0.2271	0.24503	0.41632	0.34236
Tb 350.9	0.05944	0.07196	0.09317	0.08901	0.10868	0.1194	0.18814	0.1604
Th 283.7	0.09783	0.11008	0.13717	0.13385	0.15145	0.16859	0.26626	0.23161
Tm 346.2	0.03099	0.03701	0.04782	0.04555	0.05414	0.05973	0.09323	0.08026
Y 371.02	0.0057	0.0068	0.00915	0.0091	0.01134	0.01288	0.02024	0.01906
Yb 328.9	0.00436	0.03553	0.19763	0.36546	0.8605	1.56584	1.72148	3.75483
Clay Mass (g)	0.25067	0.25168	0.2474	0.25033	0.24952	0.25207	0	0

Table A.12 Montmorillonite-Mixed REE Raw Data

C Mg/L	SM-1	SM-2	SM-3	SM-4	SM-5	SM-6	SM-7	SM-8
Ce 413.7	0.29976	0.34602	0.36191	0.46136	0.42612	0.40275	0.17895	0.57914
Dy 353.1	0.04321	0.04575	0.05055	0.06087	0.0516	0.05311	0.02845	0.07811
Er 349.9	0.08308	0.08968	0.09496	0.11634	0.0986	0.10239	0.04857	0.14171
Eu 381.9	0.01043	0.01118	0.012	0.01489	0.01265	0.01281	0.00692	0.01908
Gd 342.2	0.06614	0.06976	0.07554	0.09326	0.07904	0.08124	0.11252	0.13892
Ho 345.6	0.03369	0.03596	0.03812	0.04674	0.04052	0.04153	0.02101	0.058
La 379.4	0.04387	0.047	0.05061	0.06262	0.05351	0.05501	0.02773	0.07988
Lu 261.5	0.0048	0.00475	0.00547	0.00662	0.0056	0.0058	0.00302	0.00769
Nd 406.1	0.23511	0.25374	0.27137	0.34969	0.3104	0.29722	0.21453	0.45259
Pr 390.8	0.14102	0.15311	0.16068	0.20794	0.194	0.18829	0.09772	0.2858
Sc 361.3	0.00592	0.00616	0.00662	0.00825	0.00705	0.00718	0.00477	0.01062
Sm 442.4	0.19093	0.22338	0.23133	0.29716	0.26752	0.26915	0.12885	0.3992
Tb 350.9	0.10103	0.10633	0.11478	0.13906	0.12024	0.1222	0.05797	0.169
Th 283.7	0.14613	0.15748	0.16941	0.20285	0.17545	0.1763	0.08087	0.22743
Tm 346.2	0.04966	0.05353	0.05743	0.06882	0.05975	0.06137	0.02888	0.08321
Y 371.02	0.00982	0.01054	0.01145	0.01429	0.01187	0.01231	0.00656	0.01784
Yb 328.9	0.00535	0.00587	0.00981	0.01547	0.02226	0.02726	0.09727	0.10169
Clay Mass (g)	0.25058	0.24775	0.24998	0.25148	0.25093	0.25023	0	0

Table A.13 Ba-SY_n-1-Neodymium Raw Data

C Mg/L	BN-1	BN-2	BN-3	BN-4	BN-5	BN-6	BN-7	BN-8
Ce 413.7	0.75988	0.44662	0.57013	0.90831	0.98501	1.00916	1.33826	1.76924
Dy 353.1	0.10798	0.07786	0.11187	0.17188	0.21905	0.24772	0.29042	0.40236
Er 349.9	0.19072	0.1278	0.17848	0.27644	0.33419	0.36863	0.44706	0.6255
Eu 381.9	0.03034	0.02949	0.05116	0.07511	0.11397	0.13971	0.15403	0.22128
Gd 342.2	0.14412	0.08256	0.09926	0.16118	0.15826	0.15465	0.21633	0.28334
Ho 345.6	0.07509	0.04435	0.05379	0.08737	0.08928	0.08943	0.12107	0.16144
La 379.4	0.11371	0.08549	0.12805	0.19958	0.2606	0.3022	0.35437	0.49669
Lu 261.5	0.01038	0.00518	0.00557	0.00969	0.00839	0.0073	0.01171	0.01416
Nd 406.1	2.12292	4.89553	10.59229	14.63643	26.74803	33.49564	33.49823	50.96136
Pr 390.8	0.3847	0.2717	0.38679	0.60426	0.74521	0.84379	1.02089	1.40337
Sc 361.3	0.01487	0.00958	0.01312	0.02042	0.02475	0.02715	0.03284	0.04604
Sm 442.4	0.53242	0.30342	0.35257	0.58402	0.58377	0.56788	0.79991	1.02922
Tb 350.9	0.2197	0.11873	0.13608	0.22659	0.21145	0.19374	0.28907	0.36706
Th 283.7	0.27503	0.14552	0.16453	0.28237	0.24353	0.20495	0.33139	0.40812
Tm 346.2	0.10605	0.05766	0.06534	0.10853	0.0999	0.09205	0.13728	0.17541
Y 371.02	0.02372	0.01426	0.01856	0.02984	0.03294	0.03462	0.04445	0.061
Yb 328.9	0.01186	0.00727	0.00941	0.01506	0.01708	0.01816	0.024	0.03168
Clay Mass (g)	0.25152	0.25121	0.25111	0.25127	0.25078	0.25026	0	0

Table A.14 Ba-SYn-1-Gadolinium Raw Data

C Mg/L	BG-1	BG-2	BG-3	BG-4	BG-5	BG-6	BG-7	BG-8
Ce 413.7	0.79887	0.89767	0.36408	0.34524	0.37099	0.25916	0.31251	0.43994
Dy 353.1	0.11225	0.12772	0.06443	0.07017	0.08653	0.08199	0.09656	0.13198
Er 349.9	0.19758	0.22393	0.09691	0.10225	0.11848	0.09717	0.11756	0.15737
Eu 381.9	0.02692	0.03071	0.01395	0.01496	0.01768	0.01558	0.01865	0.02474
Gd 342.2	1.77117	5.35421	12.44881	17.49331	27.33443	36.78963	39.10994	56.51848
Ho 345.6	0.08212	0.09442	0.04659	0.05133	0.06372	0.06026	0.06991	0.0955
La 379.4	0.11421	0.1326	0.06657	0.07409	0.09197	0.08667	0.10551	0.14396
Lu 261.5	0.01079	0.01242	0.00497	0.00505	0.00586	0.00411	0.00502	0.00729
Nd 406.1	0.70113	0.9684	0.96804	1.23626	1.80652	2.20586	2.46075	3.49956
Pr 390.8	0.39117	0.46116	0.23524	0.26372	0.31711	0.3006	0.35904	0.50023
Sc 361.3	0.01472	0.01679	0.00888	0.00894	0.01078	0.00985	0.01191	0.01627
Sm 442.4	0.56965	0.64582	0.28746	0.29518	0.3332	0.27457	0.33348	0.46221
Tb 350.9	0.2418	0.27679	0.13033	0.14543	0.17475	0.1618	0.18983	0.25641
Th 283.7	0.31342	0.35023	0.14835	0.14997	0.17936	0.13395	0.15938	0.21843
Tm 346.2	0.11668	0.13548	0.06589	0.07082	0.08843	0.08216	0.08332	0.12207
Y 371.02	0.02476	0.02782	0.01197	0.01192	0.0137	0.01074	0.01321	0.01722
Yb 328.9	0.01205	0.01418	0.00729	0.00809	0.00978	0.00949	0.01117	0.01528
Clay Mass (g)	0.25161	0.25049	0.25061	0.251	0.25069	0.25043	0	0

Table A.15 Ba-SYn-1-Ytterbium Raw Data

C Mg/L	BY-1	BY-2	BY-3	BY-4	BY-5	BY-6	BY-7	BY-8
Ce 413.7	0.30648	0.28992	0.27959	0.30862	0.23101	0.377	0.32435	0.37229
Dy 353.1	0.04104	0.04248	0.04082	0.04421	0.03669	0.05849	0.04933	0.05734
Er 349.9	0.07399	0.07479	0.0706	0.0809	0.06527	0.10631	0.08853	0.10426
Eu 381.9	0.01011	0.0103	0.00971	0.01104	0.00946	0.01443	0.0123	0.0142
Gd 342.2	0.06405	0.06136	0.06065	0.07036	0.05811	0.09179	0.07997	0.09436
Ho 345.6	0.0311	0.03179	0.03307	0.03797	0.03449	0.05427	0.04683	0.05737
La 379.4	0.0416	0.04207	0.04052	0.04565	0.03602	0.05824	0.04874	0.05515
Lu 261.5	0.00362	0.00441	0.00543	0.00676	0.008	0.0117	0.01064	0.01423
Nd 406.1	0.24541	0.24587	0.21781	0.25201	0.19864	0.29728	0.27025	0.30009
Pr 390.8	0.15106	0.14613	0.14173	0.15845	0.12694	0.19154	0.17233	0.1902
Sc 361.3	0.00534	0.00548	0.00531	0.00592	0.00597	0.0082	0.00708	0.00805
Sm 442.4	0.21561	0.20968	0.19993	0.21584	0.1704	0.26535	0.23446	0.25811
Tb 350.9	0.09084	0.09814	0.09745	0.112	0.10026	0.15582	0.13484	0.16666
Th 283.7	0.11811	0.1164	0.11471	0.13818	0.1225	0.18682	0.16344	0.19531
Tm 346.2	0.04349	0.04516	0.04709	0.0541	0.04775	0.0767	0.06744	0.08093
Y 371.02	0.01052	0.01363	0.01854	0.02389	0.02917	0.04206	0.03973	0.05498
Yb 328.9	1.83462	5.74039	13.3247	19.29688	29.17382	41.30957	40.71302	58.91157
Clay Mass (g)	0.25109	0.25116	0.24969	0.25214	0.25185	0.25095	0	0

Table A.16 Ba-SYN-1-Mixed REE Raw Data

C Mg/L	BM-1	BM-2	BM-3	BM-4	BM-5	BM-6	BM-7	BM-8
Ce 413.7	0.3956	0.42382	0.48201	0.58544	0.74225	0.81044	0.81289	1.08042
Dy 353.1	0.05657	0.06538	0.08438	0.10668	0.14028	0.16646	0.16715	0.22843
Er 349.9	0.10018	0.10959	0.13705	0.17163	0.21934	0.25206	0.25614	0.34454
Eu 381.9	0.01494	0.01905	0.02795	0.03757	0.05135	0.06474	0.06615	0.09438
Gd 342.2	0.65969	1.77234	4.00459	6.05195	9.2036	12.33791	13.26815	19.18364
Ho 345.6	0.04053	0.04454	0.05373	0.06449	0.08206	0.09416	0.09485	0.12483
La 379.4	0.05932	0.0683	0.09067	0.11671	0.15703	0.18237	0.19057	0.26133
Lu 261.5	0.00501	0.00535	0.00617	0.00785	0.01015	0.01165	0.01139	0.01476
Nd 406.1	0.82757	1.85834	3.96611	5.9148	8.91658	11.84806	12.76454	18.17683
Pr 390.8	0.20571	0.2346	0.29845	0.37619	0.49987	0.5781	0.59422	0.79844
Sc 361.3	0.00735	0.00815	0.01047	0.01292	0.0168	0.02064	0.02046	0.02709
Sm 442.4	0.28501	0.29997	0.33408	0.41261	0.51092	0.55043	0.55932	0.74015
Tb 350.9	0.11956	0.12564	0.14848	0.17848	0.22168	0.24714	0.24473	0.32567
Th 283.7	0.15159	0.15722	0.17206	0.20216	0.25557	0.27828	0.27234	0.3569
Tm 346.2	0.05686	0.06221	0.07113	0.08629	0.10881	0.12059	0.12028	0.15952
Y 371.02	0.01295	0.01438	0.01885	0.02385	0.03106	0.03747	0.03748	0.05123
Yb 328.9	0.62407	1.80783	4.07347	6.41426	9.69467	13.1912	14.12103	20.34822
Clay Mass (g)	0.25059	0.25083	0.25091	0.25119	0.2511	0.24994	0	0

APPENDIX B
TIME STUDY AND RANGE STUDY

B.1 Introduction

Given that there is a lack of rare earth element (REE) data concerning the suite's interaction with clay mineral types, the purpose of the main research will be to establish the relationship between rare earth elements and clay minerals with the end goal of establishing which clays are best suited for adsorbing REE. In order to save time and conserve resources, it is in the best interest of the study to initiate a preliminary experiment that will establish the concentrations of Yb solution and weights of clay minerals to be used.

B.2 Numerical Modeling

To gain insight into the sorption of REE onto clay minerals, it is best to have two separate analyses to determine a mass balance. For this reason, experiments will be designed to have approximately half to the REE in solution to adsorb onto the clay minerals. The amount of Yb to be added is then calculated by estimating the number of surface sites for the kaolinite using methods obtained from Langmuir's 1997 textbook [21]. While it is not practical that every site will be occupied by an Yb atom, the value will act as a maximum value. From this a number of moles of Yb can be determined and then from that, a necessary concentration of Yb in the reaction solution is the final result.

$$CEC = N_S \times S_A \times 0.1661 \quad (B.1)$$

$$N_S = \frac{CEC}{S_A \times 0.1661} \quad (B.2)$$

$$TOTSA = S_A \times M_C \times 10^{18} \quad (B.3)$$

$$TOTN_S = TOTSA \times N_S \quad (B.4)$$

$$mmolesREE = \frac{TOTN_S \times 10^3}{6.0221413 \times 10^{23}} \quad (B.5)$$

$$C_{REE} = \frac{mmolesREE}{V_{H_2O}} \quad (B.6)$$

Where N_S is the number of sites per nm^2 of clay mineral, S_A is the surface area of the clay mineral, CEC is the cation exchange capacity of the clay mineral, $TOTSA$ is the total surface area of the sample, MC is the mass of the clay mineral, $TOTN_S$ is the total number of sites for the sample, and C_{Yb} is the concentration of the reacting solution to be used. As mentioned prior, the doubling of the mmoles of Yb compared to the available surface sites is there for the eventual mass balance.

B.3 Experimental Design

From the recommendations of Dr. Ranville combined with the original design suggested by Dr. Wendlandt, the experiment was comprised of a beaker filled with a REE enriched solution. The REE enriched solution used varied between 0.0067 mmoles/L and 0.67 mmoles/L to best find an acceptable value to use in the future study. The solution also contained 700 mmoles/L NaCl to serve as an electrolyte, and sodium bicarbonate to serve as a buffer. 250 mg kaolinite, obtained from the Clay Minerals Society was used as the clay mineral.

The kaolinite was placed in the beakers along with the REE enriched fluid and was agitated. After the agitation the kaolinite was removed from the beaker, centrifuged, and then the remaining fluid was analyzed via the ICP-MS in the Department of Geochemistry at the Colorado School of Mines.

The experiment was carried out at 25 °C.

pH was buffered since natural systems where a reaction similar to this may be occurring would be buffered by the host substances.

To meet standards of experimental rigor, blanks were run as well as some duplicates.

This experiment was also be used to determine the appropriate adsorption time for the experiment. The experiment and all of its variables were repeated three times, once for 12 hours, once for 24 hours, and once for 36 hours.

B.4 Hypothesis

The objective of this experiment serves to establish a basic starting concentration for a larger study of similar nature as well a standard time for clay minerals to react with the REE enriched fluids. Values obtained through the data analysis lead straight into the main study. The experiment will be viewed as successful if an isotherm can be produced from the different concentrations of Yb used.

Provided that the numerical solution is reflected in the data, when a concentration of around 0.333 mmoles/L is allowed to interact with 0.250 grams of kaolinite, the kaolinite will no longer adsorb any more Yb.

B.5 Results

The data for these series of tests shown in Figure B.1 that it does take a while for the experiments to reach equilibrium and so a higher amount of time, around 24 hours represents the minimum amount needed. It is also clear from the data that a higher REE concentration is going to be needed to achieve full saturation of the clay mineral sites than what was initially calculated. The curve should approach being level in order for equilibrium to be reached for concentration.

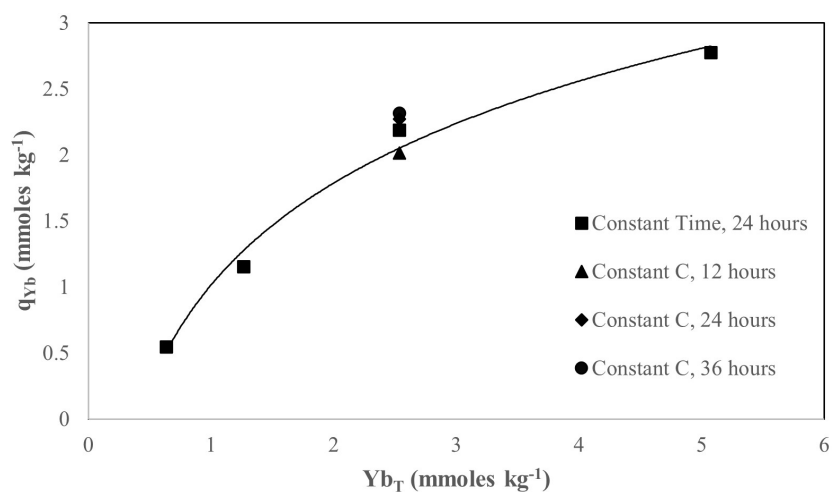


Figure B.1 This figure represents two components of the time study, a series of differing total amounts of Yb representing a constant time, 24 hours, and a constant total Yb over different times: 12, 24, and 36 hours to best understand when a reaction has reached completion

B.6 Conclusions

The parameters set forward in this experiment allowed for data to be collected and used for the purposes of the larger study that will follow this. It is clear from the data that letting the clay mineral-REE couples reach equilibrium will take time, ideally more than 24 hours. The data also show that larger concentration than what was determined will be needed to reach saturation of the clay mineral. The actual study will need to represent a larger range of concentrations than was used in this time study.

APPENDIX C

CLAY MINERAL PREPARATION

C.1 Introduction

Due to time and material constraints clay mineral samples for this project were processed with recovery yields, purity, and maintaining a specific size fraction as the main objective. Two of the clay minerals used in the project, KGa-1 and Ba-SYn-1, have been documented as being pure and procedures for processing these clay minerals are well documented in the literature [13]. On the other hand, the palygorskite and montmorillonite present challenges due to impurities and clay mineral properties. This appendix details the methods by which all clay minerals in this project were prepared for use in this study.

C.2 KGa-1

KGa-1, a kaolinite from Georgia, is extremely well documented and has been used by a number of studies cited in this thesis, but is most defined by Chipera and Bish, (2001) [13]. As has been extremely well documented, this study used the same procedures as laid out in other studies. Samples of KGa-1 were washed with a NaCl solution to strip potential chemical contaminants from the surface sites of the clay, centrifuged and left to settle, and then the samples were washed with DI water. This water was then tested with silver nitrate solution to determine if the resultant was still pulling chloride ions off of the surface sites. This process was then repeated. When it had been determined that the chloride ions had all been stripped from the surface sites of the kaolinite, the samples were then desiccated in an oven over the course of a few days. The dried clay mineral was then disaggregated using a mortar and pestle until the clay mineral was a powder that could be used in the experiment. Samples of KGa-1 were also tested by XRD to determine if their purity was at the level required for the experiment.

C.3 PFI-1

PFI-1, a palygorskite from Florida, presents challenges compared to KGa-1, in part due to its impurities and range of grain sizes. To obtain meaningful data across all PFI-1 samples, it was critical to be able to determine a pure size fraction. Any contaminants would run the risk of being more adsorptive than the clay mineral, which would invalidate the study. Thankfully, the Clay Minerals Society has determined that the impurities within the un-processed PFI-1 exist at a different size fraction than the clay mineral in question, so a simple size fractionation procedure was all that was needed to obtain a pure material to work with. Like KGa-1, PFI-1 was washed with a NaCl solution to strip any materials from the surface sites of

the clay mineral sample. This chloride enriched palygorskite was then washed heavily with DI water with the resultant being tested with silver nitrate to determine at what point the chloride had been removed. The existence of documented impurities necessitated further steps to obtain a pure sample of PFl-1. In line with Chipera and Bish (2001), obtaining palygorskite samples within the range of 0.1 to 2 μm was the goal in further processing [13]. This size fraction was isolated by using two rounds of centrifuging. The first round was used to isolate the size fraction above 2 μm . With all particles above 2 μm pulled out of suspension by the centrifuge, the supernatant containing all particles below 2 μm was removed and then centrifuged again for a longer period until all particles larger than 0.1 μm had been pulled out of suspension. The supernatant was then poured off, leaving only the 0.1 to 2 μm fraction. This was repeated several times to ensure that the material to be used in the experiment was what was desired in the initial setup. Samples were then analyzed via XRD and the results compared to the literature to ensure purity.

C.4 SWy-2

SWy-2, a montmorillonite from Wyoming, presented the most challenges of any clay mineral used in this study. The montmorillonite is well documented for swelling when subjected to water, which complicates any procedure for obtaining pure samples that uses water. Other fluids can be used, such as an alcohol, but for this experiment, the expanding properties of the montmorillonite were used to isolate pure samples. Unlike KGa-1 and PFl-1, processing SWy-2 necessitated a much more involved physical separation of the desired pure size fraction. Like the others, SWy-2 was rinsed with a NaCl solution and then cleaned using DI water, the resultant being tested with silver nitrate to determine when the wash had been complete. The samples were then centrifuged to remove the largest size fraction. As SWy-2 expands, small amounts were processed at a time to ensure that there was space for the clay mineral to be completely suspended prior to centrifuging. Large impurities were easily isolated and removed by careful centrifuging leaving the montmorillonite and other smaller particles left in suspension. This supernatant was then centrifuged under a very high rpm for a long time to drop all particles possible out of solution. The expanded montmorillonite takes on a gel-like form when compared to the other materials left over from the initial size fractionation. It is very easy to see in the column of particles brought out of suspension which fraction is the montmorillonite and which fractions are not. Obtaining a pure sample thus involves physically removing the pure montmorillonite from the other materials, being careful to only take the portion that is clearly the gel-like substance and not the grains of non-expanded material. This gel was then collected, centrifuged again to determine that was the correct size fraction, and then dried slowly over a number of days. The dried sample was then broken up with a mortar and pestle, and the results were tested with XRD to ascertain the purity of the samples. By engaging in such an involved separation

and fractionation, very pure SWy-2 was confidently obtained.

C.5 Ba-SYn-1

Unlike the other clay minerals used in the study, Ba-SYn-1 was manufactured and thus did not have the same concerns around impurities. It has also been determined by other studies to be a consistent size fraction, so much of the procedure from the other clay minerals was not applicable, leaving a very similar treatment to the KGa-1 used in this study. The Ba-SYn-1 was washed using a NaCl wash and then washed with DI water with the resultant being tested with silver nitrate to determine when the chloride had been stripped from the surface sites. The sample was centrifuged to ensure that there truly were not any undocumented impurities, and the result was then dried, and tested via XRD. One known impurity, an aluminum oxide hydroxide, was present as an artifact of the initial creation of the clay mineral, but it was determined not to have any effect on the ability for the sample to adsorb REE.